Redox Biology 39 (2021) 101811

Contents lists available at ScienceDirect

Redox Biology

journal homepage: www.elsevier.com/locate/redox

aFGF alleviates diabetic endothelial dysfunction by decreasing oxidative stress via Wnt/β-catenin-mediated upregulation of HXK2

Jia Sun [a,1], Xiaozhong Huang [b,1], Chao Niu [c,1], Xuejiao Wang [d], Wanqian Li [a], Mengxue Liu [d], Ying Wang [e], Shuai Huang [f], Xixi Chen [g], Xiaokun Li [a], Yang Wang [d,**], Litai Jin [a,***], Jian Xiao [a,****], Weitao Cong [a,*]

[a] School of Pharmaceutical Science, Wenzhou Medical University, Wenzhou, PR China
[b] Department of Pediatric Surgery, The Second Affiliated Hospital and Yuying Children's Hospital of Wenzhou Medical University, Wenzhou, PR China
[c] Pediatric Research Institute, The Second Affiliated Hospital and Yuying Children's Hospital of Wenzhou Medical University, Wenzhou, PR China
[d] Department of Histology and Embryology, Institute of Neuroscience, Wenzhou Medical University, Wenzhou, 325000, China
[e] Department of Pharmacy, Jinhua Women & Children Health Hospital, Jinhua, PR China
[f] Zhejiang Provincial Key Laboratory of Interventional Pulmonology, The First Affiliated Hospital of Wenzhou Medical University, Wenzhou, PR China
[g] Department of Pharmacy, Taizhou Central Hospital (Taizhou University Hospital), Taizhou, PR China

ARTICLE INFO

Keywords:
aFGF
Diabetes
Endothelial dysfunction
Mitochondrial superoxide
HXK2

ABSTRACT

Vascular complications of diabetes are a serious challenge in clinical practice, and effective treatments are an unmet clinical need. Acidic fibroblast growth factor (aFGF) has potent anti-oxidative properties and therefore has become a research focus for the treatment of diabetic vascular complications. However, the specific mechanisms by which aFGF regulates these processes remain unclear. The purpose of this study was to investigate whether aFGF alleviates diabetic endothelial dysfunction by suppressing mitochondrial oxidative stress. We found that aFGF markedly decreased mitochondrial superoxide generation in both db/db mice and endothelial cells incubated with high glucose (30 mM) plus palmitic acid (PA, 0.1 mM), and restored diabetes-impaired Wnt/β-catenin signaling. Pretreatment with the Wnt/β-catenin signaling inhibitors IWR-1-endo (IWR) and ICG-001 abolished aFGF-mediated attenuation of mitochondrial superoxide generation and endothelial protection. Furthermore, the effects of aFGF on endothelial protection under diabetic conditions were suppressed by c-Myc knockdown. Mechanistically, c-Myc knockdown triggered mitochondrial superoxide generation, which was related to decreased expression and subsequent impaired mitochondrial localization of hexokinase 2 (HXK2). The role of HXK2 in aFGF-mediated attenuation of mitochondrial superoxide levels and EC protection was further confirmed by si-*Hxk2* and a cell-permeable form of hexokinase II VDAC binding domain (HXK2VBD) peptide, which inhibits mitochondrial localization of HXK2. Taken together, these findings suggest that the endothelial protective effect of aFGF under diabetic conditions could be partly attributed to its role in suppressing mitochondrial superoxide generation via HXK2, which is mediated by the Wnt/β-catenin/c-Myc axis.

1. Introduction

The increasing prevalence of diabetes has become a global public health concern. In both type 1 and type 2 diabetes, glucose homeostasis is fundamentally impaired, which has a detrimental effect on cardiovascular physiology and plays an important role in the progression of many pathologies [1].

The normal artery contains three layers: an inner layer, a middle layer, and an outer layer. The inner layer is lined by a monolayer of endothelial cells (ECs) that is in contact with blood. The direct contact of ECs with the blood makes ECs highly vulnerable to damaging molecules in the blood. On the other hand, ECs form a barrier to protect the middle

* Corresponding authors.
** Corresponding author.,
*** Corresponding author.,
**** Corresponding author.
E-mail addresses: yw1867@126.com (Y. Wang), jin_litai@126.com (L. Jin), xfxj2000@126.com (J. Xiao), cwt97126@126.com (W. Cong).
[1] These authors contributed equally.

https://doi.org/10.1016/j.redox.2020.101811
Received 26 October 2020; Received in revised form 16 November 2020; Accepted 20 November 2020
Available online 19 December 2020

and outer vascular layers and adjacent tissue. In comparison with other cell types with higher energetic demand, the mitochondrial content of ECs is modest [2]. Therefore, endothelial dysfunction is an independent predictor of adverse cardiovascular outcomes [3], and damage of mitochondrial dynamics contributes to endothelial dysfunction in diverse vascular diseases [4]. In ECs, mitochondria are not only the main source of ATP, but also function as reactive oxygen species (ROS)-generating organelles [5]. Superoxide anion radical ($O_2^{\bullet-}$) and hydrogen peroxide (H_2O_2) are commonly known as the byproducts of this process [6].

Endothelial dysfunction is the earliest and most fundamental pathological change in diabetes. There is compelling evidence indicates that superoxide excess induced by diabetic hyperglycemia plays a central role in diabetic vascular cell damage [7]. High glucose flux increases the production of $O_2^{\bullet-}$ by mitochondrial electron-transport chain, and the overproduced superoxide enhances the major pathways of hyperglycemic vascular cell damage, including protein kinase C, advanced glycation end (AGE) products, and hexosamine pathways, leading to the damage of DNA, proteins, and lipids, and causes vascular cell injury [8,9]. In addition, superoxide is produced by multiple pathogenic pathways of diabetes. These include increased nicotinamide adenine dinucleotide phosphate [NAD(P)H] oxidase activity, uncoupled endothelial nitric oxide synthase (eNOS), and enhanced signaling of AGEs, angiotensin II, and oxidized-LDL receptors [10]. Thus, superoxide overproduction is considered as a major pathogenic pathway in diabetic vascular complication.

Given the fact that commonly employed antioxidants have proven ineffective in clinical trials, it is possible that these agents may not be adequately delivered to the sub-cellular sites of ROS production [10]. As the mitochondria are an important source of superoxide [11], we hypothesized that therapeutic inhibition of mitochondrial $O_2^{\bullet-}$ by a mitochondrial targeted antioxidant might be beneficial in the setting of diabetic vascular complications.

Recombinant human aFGF has been employed clinically for decades to facilitate wound/burn repair and ulcer regeneration in diabetes. However, the effects of aFGF in diabetic vascular complications are poorly defined. Previous studies identified that aFGF is upregulated by oxidative stress, implying that elevated aFGF expression is an adaptive response and may be protective in this context [12–14]. Additionally, increased endothelial resistance to oxidative stress mediated by aFGF is likely to be biologically relevant, and may open new avenues for therapeutic protection against oxidative stress [15].

In the present study, we tested the hypothesis that aFGF would alleviate diabetic vascular endothelial dysfunction by treating a type 2 diabetic mouse model with recombinant human aFGF. Our findings suggested that therapeutic inhibition of superoxide with aFGF alleviated oxidative stress and reduced pathological blood vessel changes in a mouse model of type 2 diabetes, the *db/db* mouse. Further, our findings indicated that aFGF promoted HXK2 expression via the Wnt/β-catenin/c-Myc axis, increasing mitochondrial localization of HXK2 to participate in the repair of diabetes-induced vascular endothelial injury.

2. Materials and methods

2.1. Animal procedures

C57BL/6 mice, diabetic db/db mice and their control littermates, db/m, were used for animal experiments. These mice were obtained from Model Animal Research Center of Nanjing University. The db/db mice were i.p. injected with 0.5 mg/kg body weight aFGF (produced by Key Laboratory of Biotechnology and Pharmaceutical Engineering of Zhejiang Province, Wenzhou Medical University) every other day for 8 weeks from 8 weeks of age [16]. The db/m and db/db control groups received phosphate-buffered saline (PBS; Gibco, 10010) on the same schedule as the control groups. After a 8 w course of treatment, corresponding analysis were performed. For signaling pathway analysis, each pathway antagonist: IWR (Selleck, S7086) and ICG-001 (Selleck, S2662), inhibitor of Wnt/β-catenin signaling pathway, dissolved in DMSO, were injected i.p. at 5 mg/kg right after aFGF i.p. injection [17,18]. 10058-F4 inhibitor of c-Myc (Selleck, S7153), dissolved in DMSO, was injected i.p. at 30 mg/kg right after aFGF i.p. injection [19]. 3-Bromopyruvate (3-BrPA) inhibitor of HXK2 (Sigma, 16490), dissolved in PBS, was injected i.p. at 8 mg/kg right after aFGF i.p. injection [20].

Mice were maintained at 60 ± 5% relative humidity and 22 ± 2 °C, with a 12 h light/dark cycle. All animal experimental procedures were carried out in accordance with the policies of Institutional Animal Care and Use Committee of Wenzhou Medical University, China.

2.2. In vivo wound model

General anesthesia was performed with 2% inhaled isoflurane and then injected subcutaneously with the analgesic. The hair of the back was shaved with an electric clipper followed by a depilatory cream. The skin was rinsed with alcohol and two full-thickness wounds were made using a 6-mm biopsy punch on the dorsum on each side of midline. aFGF (100 ng/mL) was injected intradermally into the wound edges in the mice, the second wound (internal control) received 50 μL of sterile PBS. For signaling pathway analysis, the wound injected with aFGF received either Ad-sh-*HXK2* solution (1×10^8 PFU prepared in 50 μL PBS) or ICG-001 (10 μM) or 10058-F4 (50 μM) or BrPA (50 μM) or cell-permeable form of hexokinase II VDAC binding domain (HXK2VBD) peptide (100 μM) (Merk, 376816) which inhibits localization of HXK2 to the mitochondrial compartment. The wounds were harvested at 7 days post wounding. Wounds were bisected on the longitudinal diameter of the wound and fixed in 10% neutral buffered formalin for CD31 immunofluorescence analyses. Inhibitors were injected intradermally into the wound edges in the mice immediately and 4 days after wounding. Ad-sh-*HXK2* solution was injected intradermally into the wound edges in the mice the day before wounding [21]. The size of wound area was photographed and measured every other day until approximately 90% of wound area was healed.

2.3. Immunofluorescence staining of mouse wound tissue

5 μm paraffin sections were cut and incubated with anti-CD31 (Abcam, ab24590). After washing, samples were incubated with Alexa fluor 647-conjugated anti-rabbit IgG secondary antibody at a dilution of 1: 200 for 60 min at room temperature. Cell nuclei were labelled by DAPI. Digital images were acquired using the Leica TCS SP5 Confocal microscope (Leica, Wetzlar, Germany).

2.4. Cell culture

HUVECs were purchased from Lonza and cultured in endothelial cell growth medium-2 (EGM-2 BulletKit, Lonza, CC-3156 & CC-4176) until the start of experiment. 5 to 7 passage subconfluent cells were used in the experiments. Before starting the experimental procedures, the medium was removed and replaced with phenol red-free low-glucose D-MEM (Gibco, 11054020) supplemented with 1% calf serum (Gibco, 16010159) for 12 h, then HUVECs were placed in EGM-2 consisting of either NG (5.5 mM) or HG (30 mM) + (PA) (0.1 mM) (HG + PA) in the presence or absence of aFGF (100 ng/mL) for 72 h, mannitol (30 mM: 5.5 mM of glucose + 24.5 mM of D-mannitol) was served as the osmotic control for the HG + PA. Media were changed every 24 h. For signaling pathway analysis, each pathway antagonist: IWR (5 μM) and ICG-001 (10 μM) was pretreated for 2 h every day before aFGF administration, HXK2VBD peptide (100 μM) (Merck, 376816) was pretreated for 1 h every day before aFGF administration.

2.5. Aortic ring assay

To establish a direct function of aFGF on vascular, thoracic aortae

from 8 w old each lines of mice were surgically isolated, cleaned, and dissected into 0.5 mm rings. Rings were embedded in 1 mg mL^{-1} of type I collagen (Millipore, 08-115) in a 96-well plate as described previously [22,23]. When embedded, the rings were cultured in serum-free endothelial basal medium (EBM) (Lonza, CC-3121) consisting of either NG (5.5 mM) or HG (30 mM) + (PA) (0.1 mM) (HG + PA) in the presence or absence of aFGF (100 ng/mL), mannitol (30 mM: 5.5 mM of glucose + 24.5 mM of D-mannitol) was served as the osmotic control for the HG + PA. For signaling pathway analysis, HXK2VBD peptide was pretreated for 1 h every day before aFGF administration, ICG-001 (10 μM) was pretreated for 2 h every day before aFGF administration. Endothelial microvessel sprouts growing out from the rings were counted during the exponential growth phase to obtain angiogenic response data. Before the regression phase, rings were fixed for immunofluorescence staining of CD31 (Abcam, ab24590). Pictures were taken on day 12, and the total number of branches was counted using ImageJ (National Institutes of Health, Bethesda, MD).

2.6. Vascular relaxation study

Measurement of isolated vascular reactivity in the organ bath is used for measuring endothelial function in mice as previously described [24]. Briefly, each aorta was separated from the surrounding connective tissue and cut into rings (3 mm). For the vasorelaxation studies, aortic rings were precontracted with an equieffective concentration of prostaglandin F2α (PGF2α) (1×10^{-6}–3×10^{-6} M). When the PGF2α-induced contraction had reached a plateau level, endothelium-dependent activators Ach (10^{-9}–10^{-5} M) or the endothelium-independent activator SNP (10^{-10}–10^{-5} M) was added in a cumulative manner.

2.7. In vitro angiogenesis (tube formation) assay

The *in vitro* angiogenic activity of HUVECs was determined by Matrigel tube formation assay. Briefly, after the experimental period described above, HUVECs were stained with cell-permeable dye, calcein (Corning, 354216), for 30 min and replated in 24-well plates precoated with 150 μL/well growth factor–reduced Matrigel (Corning, 354234) and incubated at 37 °C in cell culture incubator. After 12 h of incubation, capillary-like tube formation was observed with a computer-assisted microscope (EVOS, Thermo Fisher Scientific, MA, USA). Tube formation was defined as a tube-like structure exhibiting a length four times its width. The tube length in duplicate wells were counted and averaged using ImageJ software.

2.8. Luciferase assay

In order to determine the activation of Wnt/β-catenin signaling, the transcription factor T-cell factor/lymphoid-enhancing factor (TCF/LEF)-Luc reporter plasmid (Qiagen) was used in HUVECs. The cells were transfected with TCF/LEF-Luc reporter plasmid (SA Biosciences, Frederick, MD, USA) using lipofectamine 2000. 24 h after transfection, the cells were seeded in six-well plates at a density of 1×10^6 cells per well and treated with aFGF for 72 h. Cells were harvested and analysed for TCF/LEF activity using a luciferase assay kit (Promega-Biosciences, San Luis Obispo, CA, USA) according to the manufacturer's instruction and the activity was measured on a BioTeK Synergy HT microplate reader.

2.9. Immunoblotting analysis

Briefly, 30 μg protein from each sample was resolved by SDS–PAGE on Tris-Glycine gels, and transferred to polyvinylidene fluoride membrane. Membranes were blocked with 5% bovine serum albumin in Tris-buffered saline containing 0.1% Tween 20 (TBST) and incubated with primary antibodies overnight at 4 °C. Membranes were washed three times for 5 min with TBST, incubated in either HRP-goat-anti-mouse (Abcam, ab6789) or HRP-goat-anti-rabbit (Abcam, ab6721) secondary antibodies for 1 h at room temperature. Immunoreactive bands were visualized using Pierce ECL plus western blotting substrate (Thermo Scientific, 32132). Primary antibodies included: cleaved-Caspase-3 (Cell Signaling Technology, 9661), Bcl-2 (Abcam, ab59348), Bax (Abcam, ab32503), HXK2 (Abcam, ab209847), c-Myc (Abcam, ab32072), Cytochrome c (Cell Signaling Technology, 11940), 3-Nitrotyrosine (3-NT, Abcam, ab61392). The expression of specific antigens was quantified using ImageQuant 5.2 software (Molecular Dynamics), and the expression of GAPDH (Abcam, ab9485), Lamin B1 (Cell Signaling Technology, 12586) and COX IV (Cell Signaling Technology, 11967) were used as loading control.

2.10. Terminal deoxynucleotidyl transferase-mediated dUTP nick end labeling (TUNEL) assay

HUVECs were fixed in PBS containing 4% PFA, aortic ring from each mouse was fixed in PBS containing 4% PFA, then embedded in paraffin. The paraffinized tissues were sectioned at 5 μm and embedded on slides. Staining was performed using the In situ Cell Death Detection kit (Roche, 11684795910) in accordance with the manufacturer's protocol.

2.11. MitoSOX assay

To determine mitochondrial superoxide production in HUVECs, HUVECs were plated in six-well plate after indicated treatments. 5 mM MitoSOX solution (Thermo, M36008) was diluted to a working concentration of 1 μM with PBS. 1.0–2.0 mL of 1 μM MitoSOX reagent working solution was added to the cells. The cells were incubated for 15 min at 37 °C, protected from light, washed with buffer and then processed for imaging under a fluorescence microscope.

As for detecting aortic ring endothelial mitochondrial superoxide, briefly, unfixed segments of aortic rings were dissected in cold PBS. Surrounding tissues and intravascular blood were removed. The vessels were frozen in optimal cutting temperature compound and transverse sections (5 μm) were produced using a cryostat [25]. Sections were incubated in a 37 °C incubator for 30 min with 5 μM MitoSOX. Images were obtained with a Leica laser scanning confocal microscope with excitation/emission maxima of approximately 510/580 nm. The intensity of fluorescence signal was quantified as arbitrary units using Image J software.

2.12. Superoxide measurements using ultra-performance liquid chromatography

Cells loaded with 1 μM MitoSOX were incubated in a 37 °C incubator for 15 min. Next, buffer was aspirated, and scraped cells were mixed with methanol (200 μL) and homogenized with the cell ultrasonic disruptor. Then the samples were centrifuged for 15 min at 14000 g at 4 °C, and the supernatant were analysed by UPLC (Ultra- Performance Liquid Chromatography) according to previously published protocols [26]. MitoSOX oxidation products, 2-hydroxy-mito-ethidium and mito-ethidium, were separated using a C-18 reverse-phase column and a mobile phase containing 0.1% trifluoroacetic acid and an acetonitrile gradient (from 25% to 50%) at a flow rate of 0.3 mL/min 2-hydroxy-mito-ethidium (2-OH-Mito-E^+) and mito-ethidium (Mito-E^+) were detected with UV–Vis absorption detectors (290 nm). Production of cytoplasmic and mitochondrial $O_2^{\bullet -}$ was measured as accumulation of mito-2-hydroxyethidium in mitoSOX supplemented samples as described previously [27].

2.13. Measurement of ATP level

ATP production level was quantified in isolated mitochondria using a commercially available kit (BioVision). Briefly, tissues were lysed to free ATP into medium containing luciferase and luciferin, which produces light in the presence of ATP. The light emission is proportional to the

amount of ATP present.

2.14. Measurement of superoxide and peroxides in HUVEC

The intracellular superoxide was quantitatively measured with the Superoxide Assay Kit (S0060, Beyotime, China) to evaluate the intracellular oxidative stress level after culturing for 3 and 6 h. The culture medium was collected and diluted to a proper concentration before the assay kit was added. After cultivation for another 3 min at 37 °C, OD450 and OD600 were monitored to quantitatively determine the superoxide.

Hydrogen peroxide level was measured in cell lysates using a colorimetric assay kit according to the manufacturer instructions (Sigma Aldrich, USA, cat. No. MAK311).

2.15. TMRM staining

Mitochondrial membrane potential was measured by incubating HUVECs with TMRM (Invitrogen, T668; 25 nM) for 20 min at 37 °C. Live cells were imaged using the Leica TCS SP5 Confocal microscope (Leica, Wetzlar, Germany) and fluorescence intensity was quantified using ImageJ software. At least 30 cells were quantified per condition in replicate.

2.16. JC-1 staining

Integrity of mitochondrial membrane was assessed using JC-1 probe staining (Beyotime, C2006). HUVECs were plated in six-well plate after indicated treatments. Cells were incubated with an equal volume of JC-1 staining solution (5 μg/mL) at 37 °C for 20 min and rinsed twice with PBS. Mitochondrial membrane potentials were monitored by determining the relative amounts of dual emissions from mitochondrial JC-1 monomers or aggregates using an Olympus fluorescent microscope under Argon-ion 488 nm laser excitation. The ratio of JC-1 red/green fluorescence intensity was normalized by comparing it to the control group and is represented as loss of mitochondrial membrane potential (MMP).

2.17. Oxygen consumption rate assay

Mitochondrial oxygen consumption rate (OCR) of HUVEC was measured using the Seahorse XF96 analyser (Agilent Technologies, Santa Clara, CA), adapted from a previously described protocol [28]. 1×10^4 cells/well were equilibrated in XF Base medium (Agilent Technologies, 102353-100) supplemented with 1 mM sodium pyruvate (MilliporeSigma, S8636), 3 mM glutamine (ThermoFisher Scientific, 25030149), and 10 mM glucose (MilliporeSigma, G8769) for 1 h before addition of 2 μM oligomycin (MilliporeSigma, 75351) to measure ATP-linked respiration. Three successive additions of 1.5 μM FCCP (MilliporeSigma, C2920) were added to measure maximal respiration, with the full respiration profile obtained after addition of antimycin A (MilliporeSigma, A8674). Oxygen consumption rates were normalized against cell number.

2.18. Cell fractionation and mitochondrial isolation

Cells were homogenized in RIPA buffer (Beyotime, Nanjing, China) and the lysates were further centrifuged at 12,000 rpm for 15 min at 4 °C, then the supernatants were collected and stored at 80 °C. For cytosolic and mitochondrial proteins extraction, an isolation kit (Beyotime, Nanjing, China) was used based on manufacturer's instruction as follows. Cells were rinsed with pre-cooling PBS and gently lysed with a hypotonic buffer on ice. The lysate was disrupted by forcefully passing cells in a microfuge tube and then centrifuged at 600 g for 10 min at 4 °C to eliminate the nuclear fraction and unbroken cells. The supernatant was further centrifuged at 11,000 g for 10 min at 4 °C, the pellet was collected as the mitochondria-enriched fraction, from which the mitochondrial proteins were further resuspended in mitochondrial lysis buffer. The remaining supernatant was then centrifuged 12,000 g for 10 min at 4 °C as cytosolic proteins. Protein was estimated by Bradford assay and 30 μg was used for western blotting.

2.19. RNA isolation and semi-quantitative RT-PCR (sqRT-PCR)

Total RNA was extracted from HUVECs by using TRIzol Reagent (Invitrogen, 15596018). Next, total RNA (2 μg) was reverse transcribed into cDNA by using GoScript Reverse Transcription Kit (Promega, A5001). The cDNA was then subjected to sqRT-PCR analysis, and gene expression was quantified as previously described [25]. The mRNA levels of target genes were normalized against that of GAPDH. Gene-specific primer sequences used for qRT-PCR are listed as follows:

c-Myc
Sense 5′- CTCTCAACGACAGCAGCCCG -3′
Antisense 5′- CCAGTCTCAGACCTAGTGGA -3′
GAPDH
Sense 5′- GACCTGCCGTCTAGAAAAAC -3′
Antisense 5′- CTGTAGCCAAATTCGTTGTC -3′

2.20. Immunofluorescence staining of HUVECs and aortic ring sections

HUVECs were grown on gelatinized coverslips overnight. Briefly, after the experimental period described above. The cells were fixed in 4% paraformaldehyde in PBS for 10 min, and punched with 0.5% Triton for 15 min. The cells were then incubated with anti-β-catenin antibody (Cell Signaling Technology, 8480) overnight, followed by the Alexa Flour 647-conjugated anti-rabbit antibody (Abcam, ab150075) for 1 h at room temperature. Cellular nuclei were labelled with the fluorescent dye DAPI for 1 h. HUVECs under each experimental condition were observed under the Leica TCS SP5 Confocal microscope (Leica, Wetzlar, Germany). To evaluate HXK2 and COX IV localization, cells were treated as described above and then stained with HXK2 (Abcam, ab209847) and COX IV (Cell Signaling Technology, 11967) overnight, followed by the Alexa Flour 647-conjugated anti-rabbit antibody and Alexa fluor 488-conjugated anti-mouse IgG secondary antibody (Abcam, ab150113) at a dilution of 1: 200 for 1 h at room temperature.

For aortic ring staining, 5 μm paraffin sections were cut and incubated with anti-CD31 (Abcam, ab24590) and/or 3-NT (Abcam, ab61392). After washing, samples were incubated with Alexa fluor 647-conjugated anti-rabbit IgG secondary antibody and/or Alexa fluor 488-conjugated anti-mouse IgG secondary antibody at a dilution of 1: 200 for 60 min at room temperature. Cell nuclei were labelled by DAPI. Digital images were acquired using the Leica TCS SP5 Confocal microscope (Leica, Wetzlar, Germany).

2.21. Construction of shRNA adenoviral expression vectors

The pSilencer 2.1-U6 expression vector was purchased from Ambion (Ambion, AM5762). The U6 RNA polymerase III promoter and the polylinker region were subcloned into the adenoviral shuttle vector pDC311 (Microbix, PD-01-25). The *HXK2* shRNA targeting sequence was 5′- GCTGCTGTTCCAAGGGAAA -3'. shScramble, an in-house generated shRNA adenovirus that encodes a scramble sequence (5′-CAGTTTGGCACAATCAATA -3′), was used as control. Recombinant adenoviruses carrying the short hairpin RNA against murine *HXK2* mRNA under control of the murine vascular *Cadherin 5* core promoter were generated by homologous recombination in HEK293 cells as described previously [29].

2.22. Statistical analysis

Results are expressed as means ± SEM. Statistical differences were assessed with the unpaired 2-tailed Student's t-test for two experimental

groups and one-way ANOVA for multiple groups with SPSS software. Bonferroni's post-hoc testing was employed after ANOVA for testing for significant differences between groups. A two-tailed p value of less than 0.05 was considered statistically significant. Statistical analyses were done using GraphPad Prism (GraphPad Software).

3. Results

3.1. aFGF attenuated diabetes-induced endothelial dysfunction both in vivo and in vitro

In assessment of the protective effect of aFGF in diabetes-induced endothelial impairment *in vivo*, immunofluorescence staining for CD31 revealed the presence of de-endothelialized regions in the aortic endothelium of *db/db* mice (Fig. 1A). To further assess the endothelial function, the aortic ring assay was utilized [25]. Disrupted aortic ring sprouting function in *db/db* mice was observed compared with *db/m* littermates (Fig. 1B). Systemic treatment with aFGF (0.5 mg/kg) significantly attenuated diabetes-induced de-endothelialization and improved aortic ring sprouting compared with vehicle-treated *db/db* mice (Fig. 1A and B). We also performed organ bath studies to evaluate endothelial function and vascular response. The ACh-induced relaxation of aortic rings extracted from db/db mice was significantly weaker than that of db/m mice. This attenuated relaxation was significantly improved by aFGF treatment (Fig. 1C). In contrast, the relaxation induced by SNP showed no significantly difference among the three groups (Fig. 1C). Additionally, aortic endothelial apoptosis was increased in *db/db* mice, as demonstrated by increased TUNEL-positive cells relative to *db/m* mice, which was alleviated by aFGF treatment (Fig. 1D).

Then a direct endothelial protective role of aFGF was examined *in vitro*. Aortic rings from C57BL/6 mice were cultured in different media containing normal glucose (NG, 5.5 mM) or high glucose (HG, 30 mM) + palmitic acid (PA, 0.1 mM) (HG + PA), alone or with aFGF. In aortic rings cultured in NG medium, a well-structured microvessel network with clearly defined tubules and regular branching was present. By contrast, aortic rings cultured in HG + PA medium exhibited dramatically impaired sprouting function, which was improved by aFGF administration (Fig. 1E). In parallel, tube-forming activity was also significantly impaired in HUVECs exposed to HG + PA compared with HUVECs maintained in NG, which was significantly alleviated by aFGF co-treatment (Fig. 1F). Furthermore, HG + PA induced HUVEC apoptosis, as demonstrated by elevated Bax/Bcl-2 ratio and increased protein level of cleaved Caspase-3 (c-Caspase-3), was significantly alleviated by aFGF co-treatment (Fig. 1G). Taken together, these findings suggested a direct protective role of aFGF against diabetes-induced endothelial impairment.

3.2. aFGF decreased mitochondrial superoxide levels in vascular ECs

Mitochondrial function acts as a pivotal orchestrator of EC homeostasis under normal conditions, and mitochondrial dysfunction contributes to endothelial dysfunction in diverse vascular diseases [30]. Hence, we assessed whether aFGF could play a role in mitochondrial function. We first assessed the mitochondrial Oxygen Consumption Rate (OCR) in HUVEC. The mitochondrial respiratory reserve capacity (maximal OCR over baseline OCR) was significantly reduced in HG + PA-treated HUVEC as compared to the NG cells. In contrast, a reverse respiratory capacity was found in HG + PA-treated cells with aFGF treatment (Fig. 2A). Additionally, relative ATP production was impaired in HG + PA-treated HUVEC compared with NG cells, but greatly enhanced by aFGF treatment (Fig. 2B).

Reduced ATP production is associated with oxidative stress and mitochondrial dysfunction [31]. A large body of evidences suggest that overproduction of mitochondrial ROS (mtROS: $O_2^{\bullet-}$ and H_2O_2) leads to endothelial dysfunction and inflammation, both of which play major roles in diabetic vascular disease [32,33]. In this study, we found that aFGF significantly diminished the superoxide production in HUVEC exposed to HG + PA rather than peroxides (Figs. S1A and B), indicating that superoxide mainly mediates the effects of aFGF in regulating endothelial dysfunction.

Also, previous findings indicate that overexpression of mitochondrial superoxide dismutase (SOD2) or scavenging of mitochondrial $O_2^{\bullet-}$ with agents like mitoTEMPO improves endothelial function and reduces hypertension [34,35]. In determining the effects of aFGF on mitochondrial superoxide ($O_2^{\bullet-}$) levels *in vitro*, HUVEC were live stained with the mitochondria-specific dye MitoSOX, which becomes fluorescent upon superoxide-mediated oxidation. Then the superoxide specific product (2-OH-Mito-E^+) was measured using UPLC. As shown in Fig. 2, co-treatment with aFGF (100 ng/mL) or Mito-TEMPO (10 μM) showed the similar trends in alleviating HG + PA-induced superoxide production, as revealed by decreased fluorescence intensity of MitoSOX and reduced mitochondrial $O_2^{\bullet-}$ (Fig. 2C and D; Fig. S1D). In parallel, fluorescent staining revealed that *db/db* mice exhibited elevated mtROS levels in the aortic endothelium relative to *db/m* mice. Systemic treatment of *db/db* mice with aFGF dramatically decreased mtROS generation (Fig. 2F) in the aortic endothelium.

In addition, mitochondrial depolarization was monitored by TMRM and JC-1 staining. The results showed that treatment of HUVEC with HG + PA completely abrogated TMRM mitochondrial accumulation, along with greatly decreased JC-1 red/green fluorescence intensity ratio. By contrast, aFGF or Mito-TEMPO exposure normalized membrane potential (Fig. 2E; Fig. S1C). Meanwhile, the tube-forming activity of HUVECs exposed to HG + PA was also greatly enhanced by aFGF or Mito-TEMPO co-treatment (Fig. 2G).

The above results suggested that the protective effects of aFGF against diabetes-induced endothelial impairment might be related to its role in lowering the level of mitochondrial superoxide, but the further mechanism still need to be explored.

3.3. aFGF restored Wnt/β-catenin signaling pathway activity in diabetes, and endothelial effects of aFGF were Wnt/β-catenin-dependent

Lines of evidence support Wnt/β-catenin signaling (canonical Wnt signaling) plays an important role in ECs, ameliorating oxidative stress-induced EC apoptosis and functional impairment [36–38]. When the Wnt pathway is activated, β-catenin escapes degradation and translocates to the nucleus to form transcriptionally active complexes with sequence-specific DNA-binding T-cell factor/lymphoid enhancer factor (TCF/LEF)-family proteins, activating target gene expression [39,40]. To explore the possible mechanism for the protective effects of aFGF in HG + PA-induced endothelial injury, we first isolated nuclear and cytosolic extracts of HUVECs, then the nuclear translocation of β-catenin was analysed by immunofluorescence and immunoblotting. Nuclear translocation of β-catenin was significantly decreased in HUVECs exposed to HG + PA but partially restored by aFGF co-treatment (Fig. 3A and B).

To determine whether the Wnt/β-catenin pathway played an important role in the endothelial protective effects of aFGF, the Wnt pathway was blocked by treatment with IWR and ICG-001, that promote β-catenin degradation and antagonize β-catenin/TCF/LEF-mediated transcription, respectively. Inhibition of Wnt/β-catenin signaling with IWR counteracted aFGF-mediated β-catenin nuclear translocation (Fig. 3A and B). Meanwhile, IWR and ICG-001 both inhibited aFGF-modulated increase of mitochondrial respiratory reserve capacity and ATP production (Fig. 3C and D). and increased aFGF-modulated suppression of superoxide production (Fig. 3E and F) and mitochondrial depolarization (Fig. 3G; Fig. S2A). In parallel, TUNEL-positive cells were significantly increased by both IWR and ICG-001 co-treatment with aFGF (Fig. 3H), along with damaged tube-forming activity (Fig. 3I) compared with HUVECs maintained in only aFGF co-treatment.

The functional role of the Wnt/β-catenin pathway in aFGF-mediated

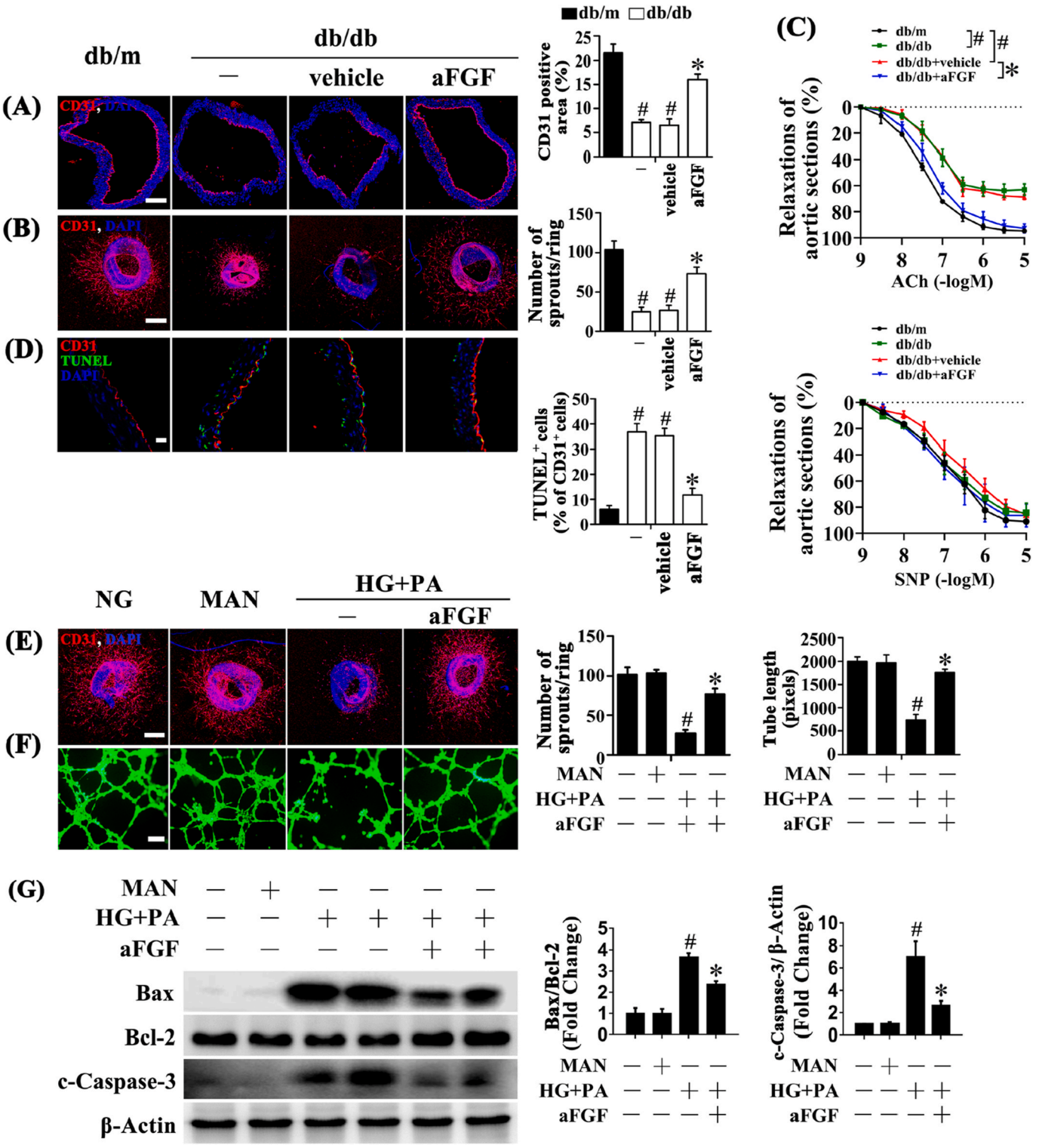

Fig. 1. aFGF attenuated diabetes-induced endothelial dysfunction both *in vivo* and *in vitro*. (**A**) Representative immunofluorescence with CD31 of aorta tissue sections, scale bars = 200 μm. (**B**) Representative confocal images of aortic rings sprouting, scale bars = 500 μm. (**C**) Concentration–response curves following Ach or SNP treatments of mice aortic rings. (**D**) Representative confocal images of TUNEL stained aorta tissue sections, scale bars = 20 μm, from db/m mice, db/db mice, and intraperitoneal aFGF (0.5 mg/kg) treated db/db mice aorta tissue sections. (**E**) Capillary-like tube formation of HUVECs, scale bars = 300 μm, HUVECs were cultured either in NG or HG + PA medium in the presence or absence of aFGF (100 ng/mL) for 72 h, MAN was served as the osmotic control for the HG + PA. (**F**) Representative confocal images of aortic rings sprouting, scale bars = 500 μm. (**G**) Cell lysates of HUVECs were used to detect the Bax, Bcl-2 as well as c-Caspase-3 protein levels by immunoblotting. β-Actin was served as the loading control. All values displayed are means ± SEM of 6 independent experiments. For (A)-(D), #p < 0.05 vs. db/m mice; *p < 0.05 vs. db/db mice or vehicle treated db/db mice; For (E)-(G), #p < 0.05 vs. NG or MAN; *p < 0.05 vs. HG + PA.

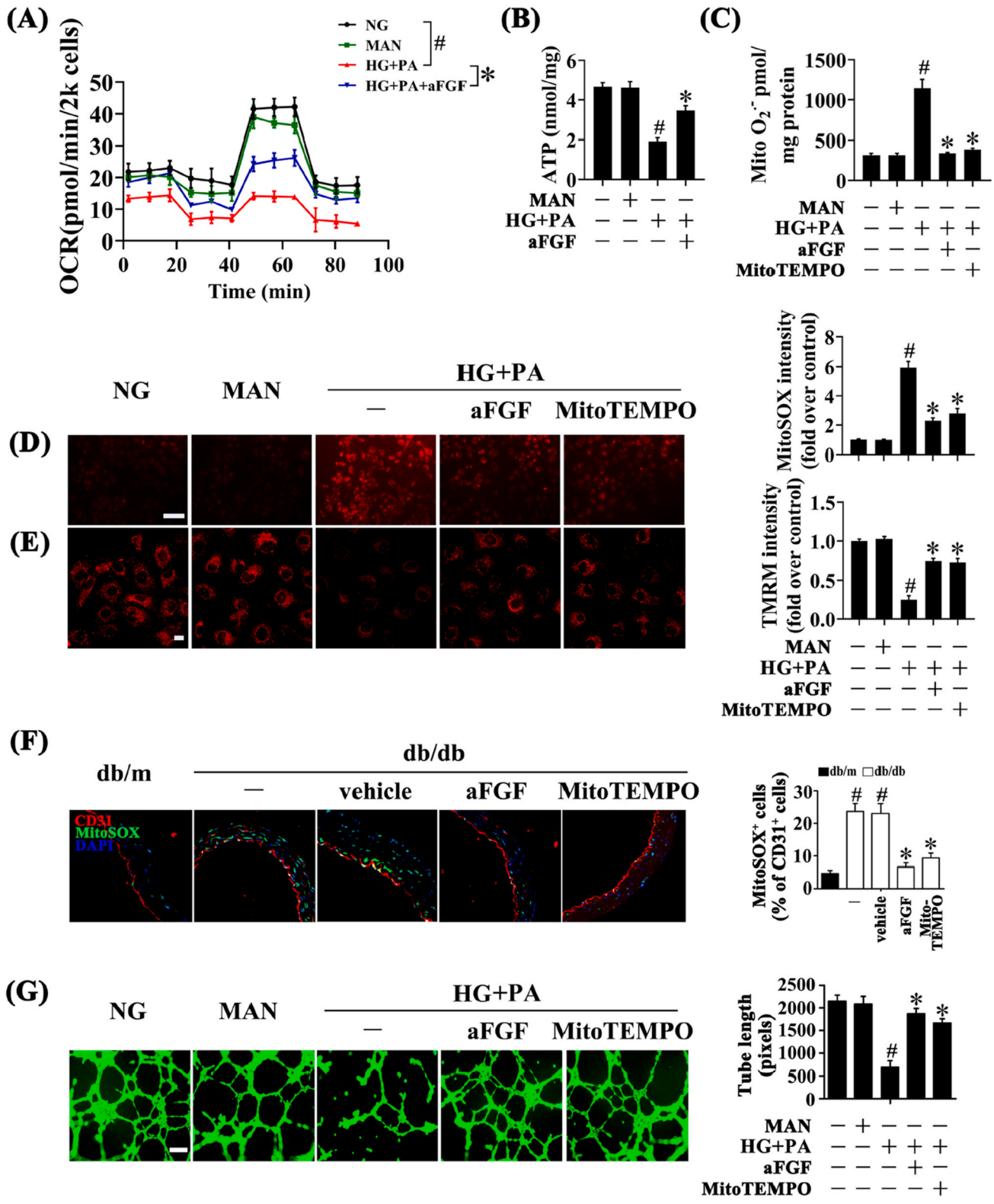

Fig. 2. aFGF lowered the level of mitochondrial superoxide in vascular endothelial cells. (**A**) OCR was analysed using a Seahorse XF analyser. (**B**) ATP production in HUVEC. (**C**) Mitochondrial $O_2^{\bullet-}$ in HUVEC was measured by mitochondria targeted probe MitoSOX and UPLC after accumulation of $O_2^{\bullet-}$-specific product 2-OH-Mito-E^+. (**D**) mtROS of HUVECs was detected by MitoSOX staining assay, scale bars = 1000 μm. HUVECs were cultured either in NG or HG + PA medium in the presence or absence of aFGF (100 ng/mL) or MitoTEMPO (10 μM) for 72 h. MAN was served as the osmotic control for the HG + PA. (**E**) Mitochondrial membrane potential of HUVECs was detected by TMRM fluorescence staining, scale bars = 5 μm. (**F**) Representative confocal images of MitoSOX stained aorta tissue sections, scale bars = 20 μm, from db/m mice, db/db mice, and intraperitoneal aFGF (0.5 mg/kg) or MitoTEMPO (0.7 mg/kg) treated db/db mice. (**G**) Capillary-like tube formation of HUVECs, scale bars = 300 μm. All values displayed are means ± SEM of 6 independent experiments. For (A)-(E) and (G), #p < 0.05 vs. NG or MAN; *p < 0.05 vs. HG + PA; For (F), #p < 0.05 vs. db/m mice; *p < 0.05 vs. db/db mice or vehicle treated db/db mice.

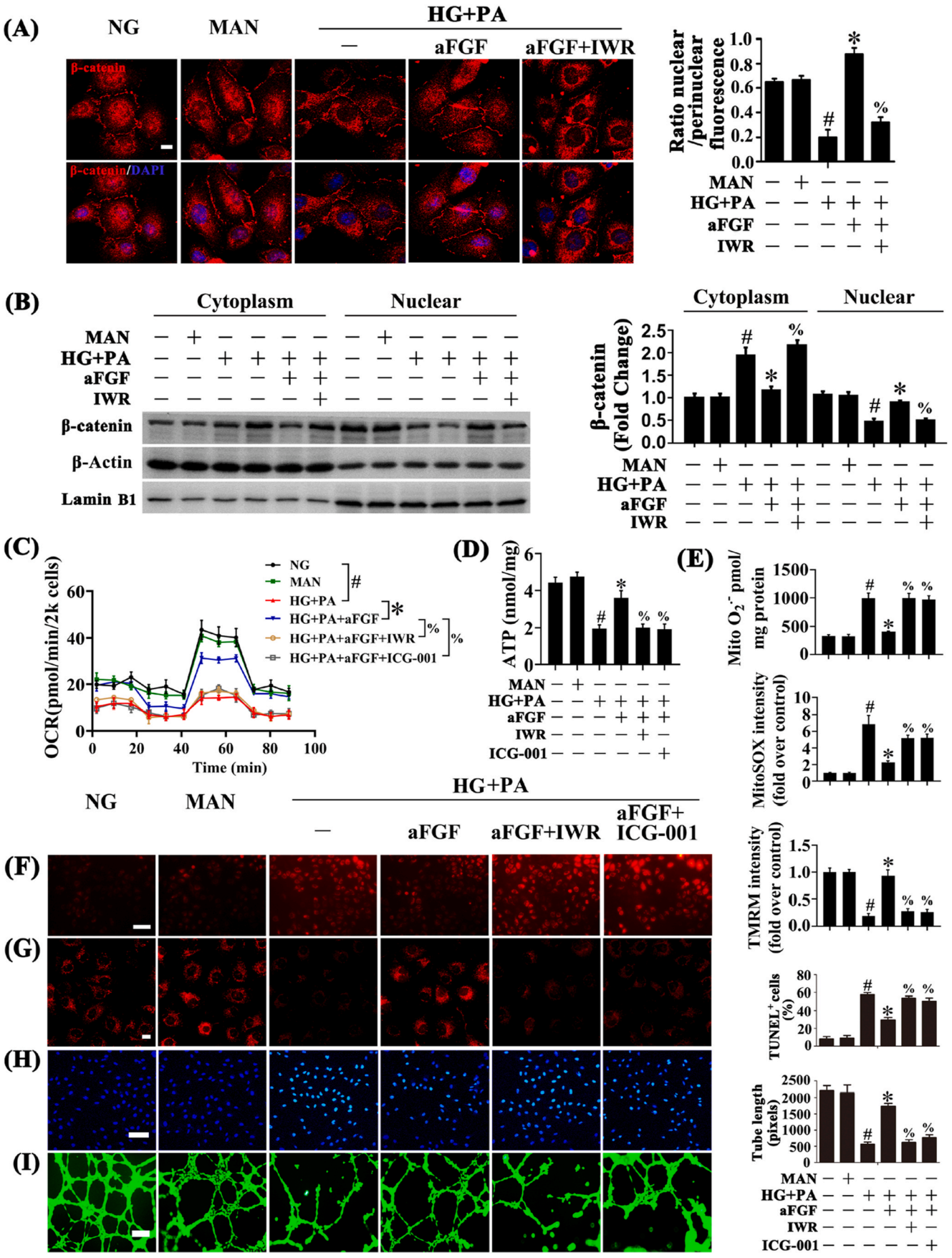

(caption on next page)

Fig. 3. aFGF restored HG + PA-reduced Wnt/β-catenin signaling pathway activity, and the endothelial protective action of aFGF against HG + PA is Wnt/β-catenin signaling pathway dependent, *in vitro*. (**A**) Representative immunofluorescence staining with β-catenin in HUVECs, scale bars = 5 μm, (**B**) Nuclear and cytosolic extracts from HUVECs were isolated to detect β-catenin protein level by immunoblotting. Lamin B1 and β-Actin were served as loading controls for nuclear and cytosolic fractions, respectively, HUVECs were cultured either in NG or HG + PA medium alone or with aFGF (100 ng/mL) for 72 h, MAN was served as the osmotic control for the HG + PA. For manipulation of Wnt/β-catenin pathway, IWR (5 μM) was pretreated for 2 h before aFGF administration. (**C**) OCR was analysed using a Seahorse XF analyser. (**D**) ATP production in HUVEC. (**E**) Mitochondrial $O_2^{\bullet-}$ in HUVEC was measured by mitochondria targeted probe MitoSOX and UPLC after accumulation of $O_2^{\bullet-}$-specific product 2-OH-Mito-E$^+$. (**F**) mtROS of HUVECs was detected by MitoSOX staining assay, scale bars = 1000 μm, (**G**) Mitochondrial membrane potential was detected by TMRM fluorescence staining, scale bars = 5 μm, (**H**) TUNEL assay of HUVECs, scale bars = 100 μm, (**I**) Capillary-like tube formation of HUVECs, scale bars = 300 μm. All values displayed are means ± SEM of 6 independent experiments. #$p < 0.05$ vs. NG or MAN; *$p < 0.05$ vs. HG + PA; % $p < 0.05$ vs. HG + PA co-incubated with aFGF.

diabetic endothelial protection was further verified by *in vivo* experiments. We directly delivered IWR or ICG-001 through intraperitoneal injection to block the Wnt/β-catenin pathway. IWR and ICG-001 both largely counteracted aFGF-modulated endothelial protection in *db/db* mice, as demonstrated by decreased relaxation of aortic sections (Fig. S2B), dramatically increased de-endothelialized regions (Fig. S2C), increased mtROS generation (Fig. S2D), together with significantly increased TUNEL-positive cells in the aortic endothelium (Fig. S2E) in *db/db* mice.

3.4. aFGF activated Wnt/β-catenin signaling pathway to promote c-Myc expression and protected the endothelial function against HG + PA

To determine if aFGF-induced β-catenin translocation could alter gene expression via TCF/LEF cis-elements, a luciferase reporter vector containing TCF/LEF cis-elements regulating luciferase expression was transfected into HUVECs. Transcriptional activity of TCF/LEF was significantly decreased in HUVECs exposed to HG + PA but greatly increased by aFGF co-treatment. However, in the presence of IWR or ICG-001, aFGF-mediated activation of TCF/LEF transcription was blocked (Fig. 4A).

Next, we explored the potential downstream target genes of aFGF-mediated Wnt/β-catenin activation. The oxidation-sensitive transcription factor c-Myc is a known Wnt/β-catenin target gene [41], which could enhance mitochondrial functional capacity, thus playing an important role in ECs [42,43]. In HUVECs exposed to HG + PA, both transcriptional and protein levels of c-Myc were significantly decreased, but were restored by aFGF co-treatment. However, in the presence of IWR or ICG-001, aFGF-mediated upregulation of c-Myc was attenuated (Fig. 4B).

To clarify the role of c-Myc in regulating aFGF-mediated endothelial protection against HG + PA, we used si-*c-Myc* to disrupt c-Myc expression in HUVECs. In the presence of si-*c-Myc*, aFGF-modulated endothelial protective effects were largely abolished, as indicated by decreased mitochondrial respiratory reserve capacity, ATP production, and dramatically increased superoxide generation (Fig. 4E and F) and mitochondrial depolarization (Fig. 4G; Fig. S3A), concomitant with increased TUNEL-positive cells (Fig. 4H) and impaired tube-forming activity in HUVECs (Fig. 4I).

3.5. aFGF promoted c-Myc expression to increase HXK2 expression and mitochondrial localization

The proto-oncogene c-Myc has been reported to regulate the expression of HXK2, a key enzyme for integrating energy production and cell viability [44]. c-Myc upregulates HXK2, which becomes enriched and associated with the mitochondrial voltage-dependent anion channel (VDAC), leads to inhibition of competing apoptotic signals for binding to VDAC [45]. By contrast, cells lacking HXK2 forces the chance of electron leaking increase, resulting in enhanced ROS and superoxide anion production [46]. Therefore, we investigated the possible role of c-Myc in aFGF regulation of HXK2 expression. Western blot analysis demonstrated that aFGF restored HG + PA impairment of HXK2 expression, while si-*c-Myc* (Fig. S4A) as well as si-*Hxk2* (Fig. S4B) prevented aFGF-induced upregulation of HXK2.

To gain insight into the involvement of HXK2 in aFGF-mediated endothelial protection, we determined the role of aFGF in the regulation of mitochondrial HXK2 localization. aFGF restored HG + PA-downregulated HXK2 expression and subsequently promoted mitochondrial HXK2 localization, as demonstrated by increased mitochondrial binding of HXK2 (Fig. 5A), concomitant with increased co-staining of HXK2 puncta (red) with COX IV (green) (Fig. 5B). Moreover, aFGF also prevented HG + PA-induced Cytochrome C release from mitochondria into the cytosol (Fig. 5A). To further clarify the role of HXK2 in aFGF-mediated endothelial protection, we used si-*Hxk2* to interfere with the expression of HXK2 in HUVECs. In the presence of si-*Hxk2*, aFGF could no longer induce HG + PA-impaired HXK2 expression and its further combination with mitochondria (Fig. 5A and B), accompanied with the release of Cytochrome C from mitochondria to the cytosol (Fig. 5A). Also, aFGF-modulated endothelial protective effects were largely attenuated by si-*Hxk2*, which exhibited decreased mitochondrial respiratory reserve capacity and ATP production (Figs. S4C and D), consistent with increased superoxide generation (Fig. 5C; Fig. S4E), mitochondrial depolarization (Fig. 5D; Fig. S4F), and TUNEL-positive cells in HUVECs (Fig. 5E), along with damaged tube-forming activity of HUVECs (Fig. 5F).

The functional role of c-Myc and HXK2 in aFGF-mediated diabetic endothelial protection was further confirmed in *db/db* mice. The c-Myc inhibitor 10058-F4 and the HXK2 inhibitor 3-BrPA were intraperitoneally injected respectively, in mice co-treated with aFGF. Both 10058-F4 and 3-BrPA counteracted aFGF-modulated endothelial protection in *db/db* mice, as demonstrated by decreased relaxation of aortic sections (Fig. S5E), increased de-endothelialized regions (Fig. S5A), and increased mtROS generation (Fig. S5B) in the aortic endothelium. In parallel, TUNEL-positive cells were significantly increased by both 10058-F4 and 3-BrPA co-treatment (Fig. S5D).

3.6. aFGF promoted the combination of HXK2 with mitochondria to protect endothelial function against HG + PA

As, increased HXK2 expression contributes to the coupling between HXK2 and mitochondria, thus protecting cells from mitochondrial oxidative stress [45,46]. We next explored the functional role of HXK2 mitochondrial localization in regulating aFGF-mediated endothelial protection. We used HXK2VBD to disrupt mitochondrial localization of HXK2 in HUVECs. In the presence of HXK2VBD, aFGF alleviated HG + PA impairment of HXK2 expression but no longer promoted mitochondrial localization of HXK2 (Fig. 6A, E), accompanied by increased release of Cytochrome C from mitochondria to the cytosol (Fig. 6A). Consequently, aFGF-modulated endothelial protective effects were largely attenuated by HXK2VBD, as demonstrated by decreased mitochondrial respiratory reserve capacity and ATP production (Fig. 6B and C), increased superoxide production (Fig. 6D, F), increased mitochondrial depolarization (Fig. 6G; Fig. S3B), increased TUNEL-positive HUVECs (Fig. 6E), and disruption of tube-forming activity (Fig. 6F).

3.7. Inhibition of the Wnt/β-catenin/c-Myc/HXK2 axis disrupted aFGF-mediated wound healing in db/db mice

Vascular endothelial dysfunction contributes to many diabetic

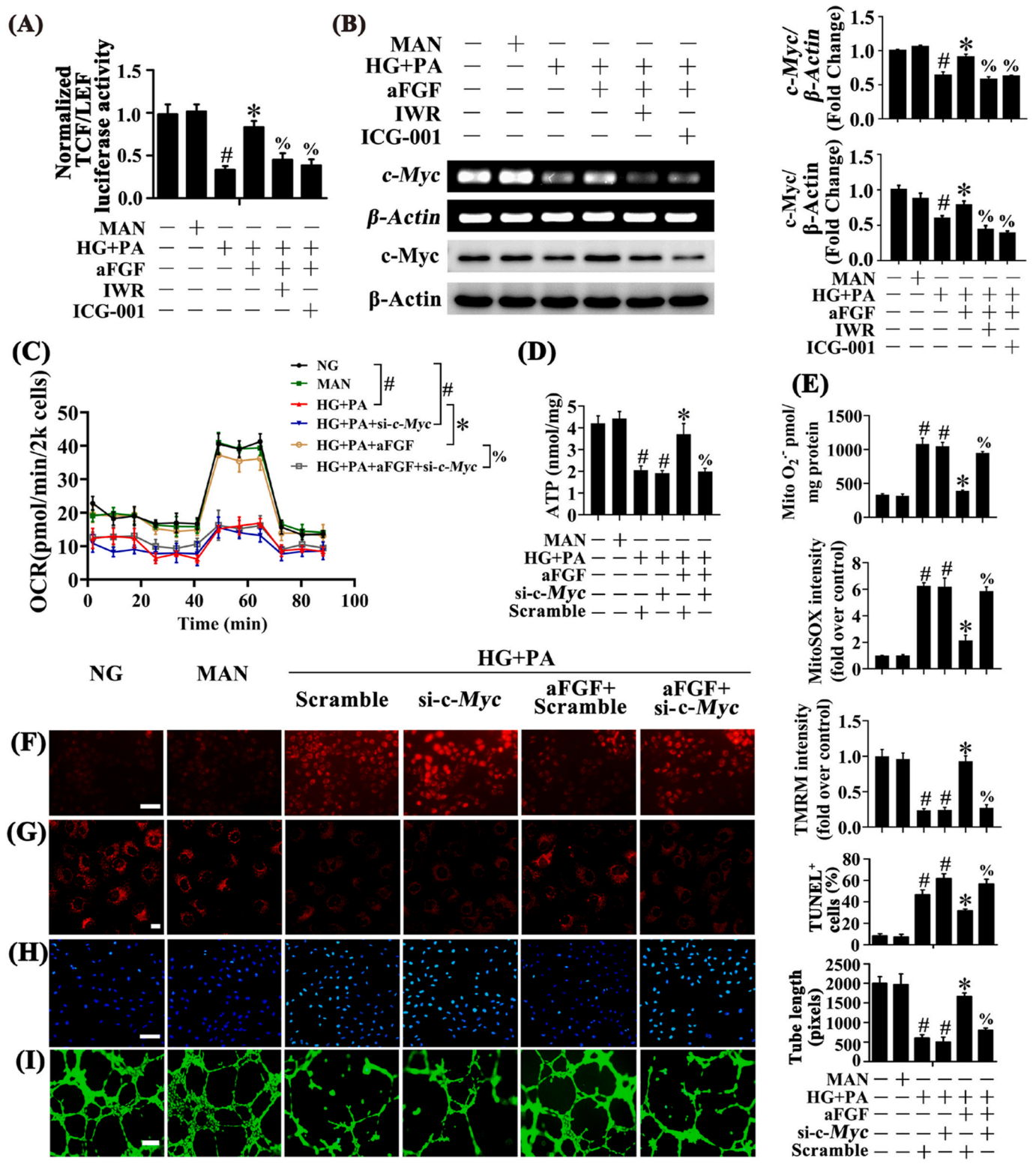

Fig. 4. aFGF activated Wnt/β-catenin signaling pathway to promote c-Myc expression and protect the endothelial function against HG + PA. (**A**) TEF/LEF-luciferase reporter activity in HUVECs. (**B**) Immunoblotting and sqRT-PCR analysis of c-Myc in HUVECs. HUVECs were cultured either in NG or HG + PA medium in the presence or absence of aFGF (100 ng/mL) for 72 h, MAN was served as the osmotic control for the HG + PA. For manipulation of Wnt/β-catenin pathway, IWR (5 μM) and ICG-001 (10 μM) was pretreated for 2 h before aFGF administration. (**C**) OCR was analysed using a Seahorse XF analyser. (**D**) ATP production in HUVEC. (**E**) Mitochondrial $O_2^{\bullet-}$ in HUVEC was measured by mitochondria targeted probe MitoSOX and UPLC after accumulation of $O_2^{\bullet-}$-specific product 2-OH-Mito-E^+. (**F**) mtROS of HUVECs was detected by MitoSOX staining assay, scale bars = 1000 μm, (**G**) Mitochondrial membrane potential was detected by TMRM fluorescence staining, scale bars = 5 μm, (**H**) TUNEL assay of HUVECs, scale bars = 100 μm, (**I**) Capillary-like tube formation of HUVECs, scale bars = 300 μm. All values displayed are means ± SEM of 6 independent experiments. #$p < 0.05$ vs. NG or MAN; *$p < 0.05$ vs. HG + PA; % $p < 0.05$ vs. HG + PA co-incubated with aFGF.

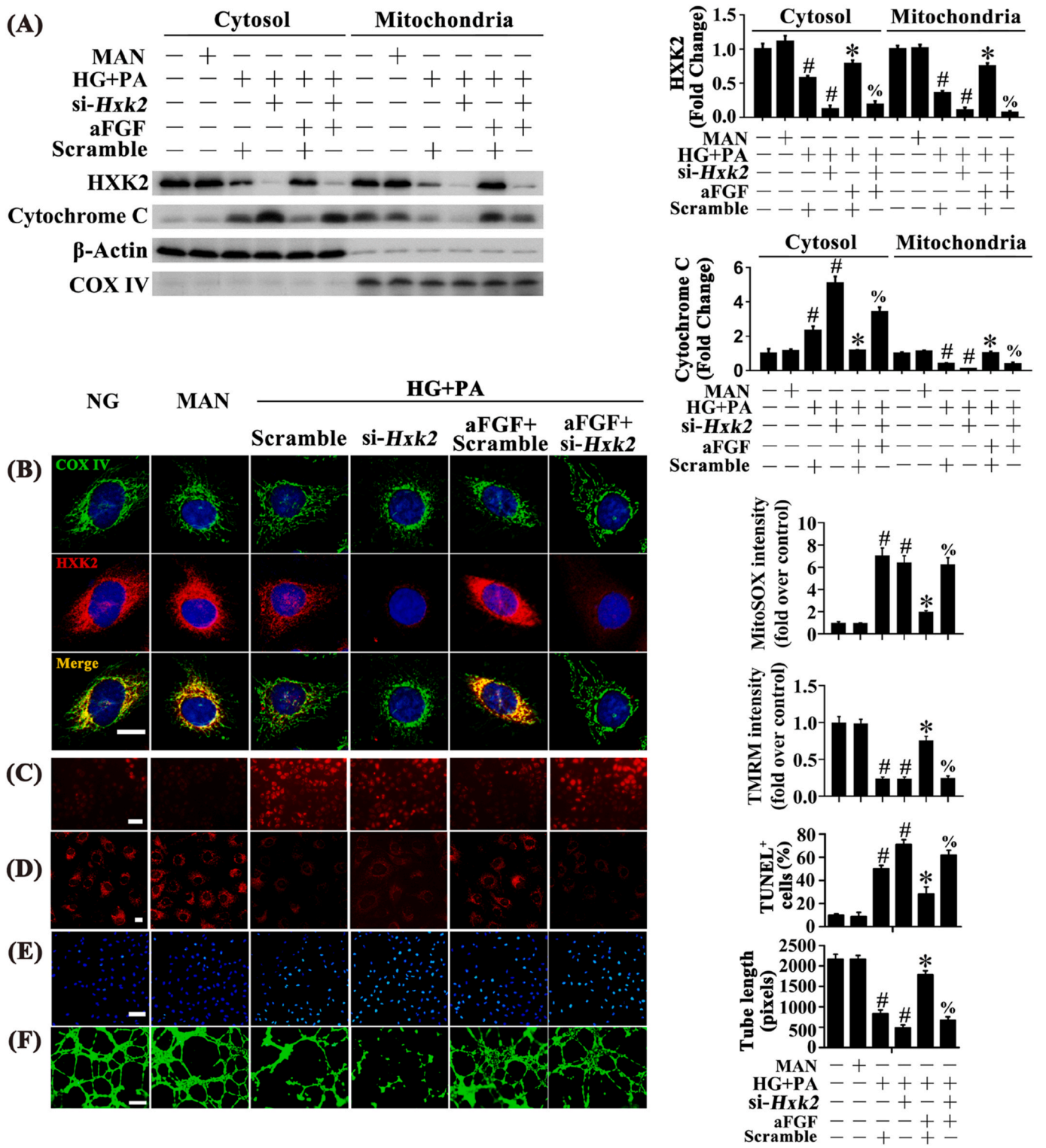

Fig. 5. aFGF promoted c-Myc expression to increase HXK2 expression and its mitochondrial localization. (**A**) Mitochondrial and cytosolic extracts were isolated to detect the HXK2 and Cytochrome c protein levels in HUVECs. COX IV and β-Actin were served as loading controls for mitochondrial and cytosolic fractions, respectively. (**B**) Representative immunofluorescence analysis of HXK2 (red) in HUVECs. The COX IV immunostaining (green) highlights mitochondria, and nuclei were stained with DAPI (blue), scale bars = 5 μm, (**C**) mtROS of HUVECs was detected by MitoSOX staining assay, scale bars = 1000 μm, (**D**) Mitochondrial membrane potential was detected by TMRM fluorescence staining, scale bars = 5 μm, (**E**) TUNEL assay of HUVECs, scale bars = 100 μm, (**F**) Capillary-like tube formation of HUVECs, scale bars = 300 μm. All values displayed are means ± SEM of 6 independent experiments. #$p < 0.05$ vs. NG or MAN; *$p < 0.05$ vs. HG + PA; % $p < 0.05$ vs. HG + PA co-incubated with aFGF. (For interpretation of the references to color in this figure legend, the reader is referred to the Web version of this article.)

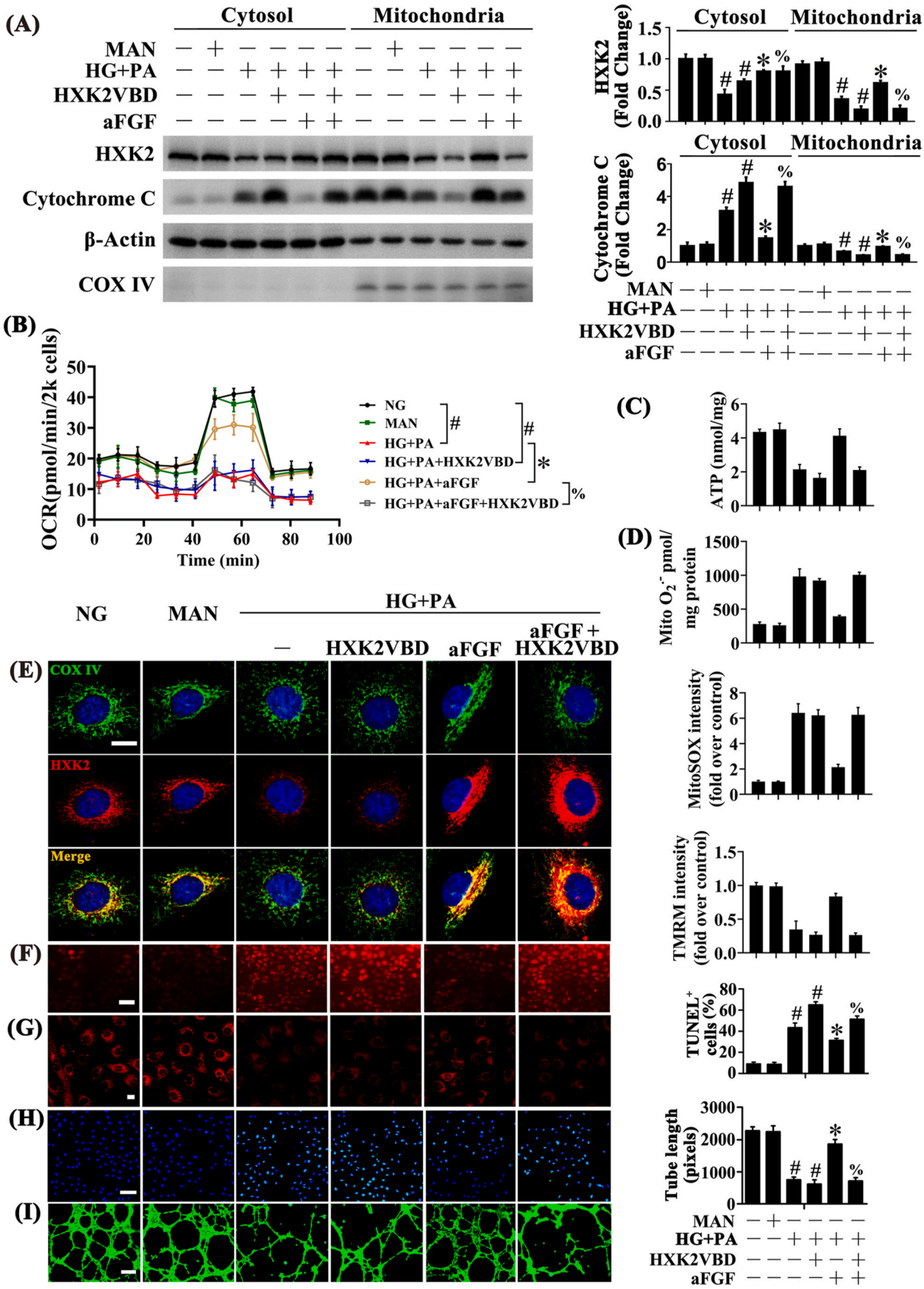

(caption on next page)

Fig. 6. aFGF promoted the combination of HXK2 with mitochondria to protect the endothelial function against HG + PA. (**A**) Mitochondrial and cytosolic extracts were isolated to detect the HXK2 and Cytochrome c protein levels in HUVECs. HUVECs were cultured either in NG or HG + PA medium alone or with aFGF (100 ng/mL) for 72 h, MAN was served as the osmotic control for the HG + PA, cell-permeable form of HXK2VBD (100 μM) was pretreated for 1 h before aFGF administration. (**B**) OCR was analysed using a Seahorse XF analyser. (**C**) ATP production in HUVEC. (**D**) Mitochondrial $O_2^{\bullet-}$ in HUVEC was measured by mitochondria targeted probe MitoSOX and UPLC after accumulation of $O_2^{\bullet-}$-specific product 2-OH-Mito-E^+. (**E**) Representative immunofluorescence analysis of HXK2 (red) in HUVECs. The COX IV immunostaining (green) highlights mitochondria, and nuclei were stained with DAPI (blue), scale bars = 5 μm, (**F**) mtROS of HUVECs was detected by MitoSOX staining assay, scale bars = 1000 μm, (**G**) Mitochondrial membrane potential was detected by TMRM fluorescence staining, scale bars = 5 μm, (**H**) TUNEL assay of HUVECs, scale bars = 100 μm, (**I**) Capillary-like tube formation of HUVECs, scale bars = 300 μm. All values displayed are means ± SEM of 6 independent experiments. #$p < 0.05$ vs. NG or MAN; *$p < 0.05$ vs. HG + PA; %$p < 0.05$ vs. HG + PA co-incubated with aFGF. (For interpretation of the references to color in this figure legend, the reader is referred to the Web version of this article.)

complications, including impaired wound healing [47]. Therefore, we examined the functional role of the Wnt/β-catenin/c-Myc/HXK2 pathway *in vivo* using a mouse skin wound healing model in *db/db* mice. Wound healing was defective in *db/db* mice, which was accompanied by decreased c-Myc and HXK2 expression in skin lysates. aFGF promoted wound healing, and upregulated HXK2 and c-Myc expression (Fig. S6A). We then examined the functional role of aFGF-mediated upregulation of c-Myc and HXK2. aFGF restored $CD31^+$ capillary density in skins of *db/db* mice, which was abrogated by IWR, 10058-F4, or 3-BrPA co-treatment (Fig. 7A). Meanwhile, aFGF acceleration of wound healing in *db/db* mice was also abolished by these inhibitors (Fig. 7B).

Furthermore, *Hxk2* was specifically knocked down in *db/db* skin wound endothelia using a FLAG-tagged adenovirus carrying short hairpin RNA against murine *Hxk2* mRNA under control of the murine vascular endothelial (VE)-*Cadherin 5* core promoter (EC-sh-*Hxk2*). Specificity was confirmed in EC-sh-*Hxk2*-transfected HUVECs and 3T3 cells by detecting the expression of Flag protein (Fig. S6B). EC-sh-*Hxk2* dramatically abolished aFGF-mediated HXK2 increase in the regenerative skin tissue of wounds from *db/db* mice (Fig. S6C). Meanwhile, aFGF restoration of $CD31^+$ capillary density (Fig. 7C) and acceleration of wound healing in *db/db* mice were abrogated by endothelial *Hxk2* knockdown (Fig. 7D).

To further clarify the role of HXK2 mitochondrial localization in the regulation of aFGF-mediated diabetic endothelial protection *in vivo*, we used HXK2VBD to interfere with mitochondrial location of HXK2 in wound sites of *db/db* mice. In the presence of HXK2VBD, aFGF still alleviated the impairment of HXK2 expression in diabetes (Fig. S6C). Nevertheless, HXK2VBD almost entirely restrained aFGF-restored $CD31^+$ capillary density (Fig. 7C) and accelerated wound healing in *db/db* mice (Fig. 7D).

4. Discussion

The present study provides novel evidence that the endothelial protective effects of aFGF in diabetes are due in part to alleviation of diabetes-induced superoxide increase. This effect was modulated by upregulation of c-Myc expression through the Wnt/β-catenin axis, and subsequent increase of HXK2 expression and localization to mitochondria.

To alleviate diabetic complications, several large trials targeted the commonly accepted risk factors for diabetic complications, including hyperglycemia, hypertension, and hyperlipidemia. Unfortunately, none of the trials successfully reduced the primary endpoints of cardiovascular morbidity and mortality [48,49]. Novel approaches to improve these outcomes are an urgent unmet clinical need. The development of new treatments has largely been guided by the concept that oxidative stress, primarily driven by mitochondrial superoxide, underlies diabetic complications [32,50]. Thus, landmark publications, indicating that mitochondrial production of superoxide is a unifying mechanism that regulates the major pathways of diabetic complications, including polyol flux, protein kinase C, advanced glycosylation end products, and hexosamine flux, were widely accepted [7,32,51]. Our findings demonstrated that aFGF efficiently inhibited mitochondrial superoxide generation in HG + PA-exposed HUVECs, and abolished diabetes-induced mitochondrial superoxide production and oxidative damage in the aortic endothelium. Of note, aFGF improved mitochondrial respiration in endothelial cells under diabetic conditions. Considering the fact that mitochondria may possess multiple pathways to help minimize glucose-induced oxidative stress and that hyperglycemia can alter the mitochondrial respiration independent of superoxide generation [52], the endothelial protective effect of aFGF under diabetic conditions could be associated with improved mitochondrial metabolic function.

aFGF is a multifunctional protein and is protective against many types of stress [53]. Prior studies identified that aFGF is upregulated by oxidative stress, implying that increased aFGF expression is an adaptive response and could protect against oxidative stress [13–15]. Also, prior findings demonstrated that aFGF alleviates diabetic testicular cell death and prevents diabetic cardiomyopathy, and that both effects are likely modulated by alleviation of diabetic oxidative stress [54,55]. In the present study, we demonstrated that therapeutic inhibition of mtROS with aFGF prevented oxidative stress and reduced pathological blood vessel changes in type 2 diabetes, which was dependent on Wnt/β-catenin signaling.

The pleiotropic effects of Wnt/β-catenin signaling are well-established, with known roles in cardiovascular development, regeneration, and angiogenesis [56]. However, the role of Wnt/β-catenin signaling in oxidative stress regulation appears to be context-dependent. For example, Wnt/β-catenin signaling protected against hepatic ischemia/reperfusion injury and decreased ROS levels, and loss of β-catenin triggers oxidative stress and impairs hematopoietic regeneration in this model [57]. On the contrary, β-catenin deficiency or Wnt/β-catenin inhibition is beneficial in cardiac ischemic injury [58]. Therefore, the precise mechanisms of the Wnt/β-catenin pathway and its regulatory roles in oxidative stress should be assessed under specific circumstances. In the present study, overproduction of mtROS in the vascular endothelium of diabetic mice and HUVECs exposed to HG + PA were observed, driven in part by inhibition of the Wnt/β-catenin pathway. aFGF abolished diabetes-induced mtROS production and oxidative damage in ECs by activating Wnt/β-catenin signaling.

c-Myc, as a Wnt/β-catenin downstream target gene, is an oxidation-sensitive transcription factor [41,59]. Suppression of c-Myc expression depletes cellular ATP levels, enhances oxidative stress, promotes mitochondrial dysfunction, and causes significant DNA damage, resulting in apoptosis [60]. In this study, transcription and protein expression analyses of c-Myc in HG + PA-exposed HUVECs, in the presence or absence of aFGF, revealed that aFGF markedly restored HG + PA-mediated decrease of c-Myc levels. To elucidate the roles of c-Myc in the endothelial protective effects of aFGF, we used si-*c-Myc* to disrupt expression of c-Myc in HUVECs. In the absence of c-Myc, aFGF-modulated endothelial protective effects were largely abolished. This result was further confirmed *in vivo* by treating *db/db* mice with the c-Myc inhibitor 10058-F4, which abolished the endothelial protective effects of aFGF.

HXK2, a c-Myc transcriptional target, contains a mitochondria-targeting domain [45] that localizes the enzyme to the VDAC/adenine nucleotide translocase channel. Silencing of *Hxk2* significantly decreased mitochondrial localization of HXK2, subsequently enhancing mtROS production [46]. c-Myc knockdown decreases HXK2 mRNA and protein levels in HUVECs, while c-Myc overexpression upregulates HXK2 [61]. In addition to upregulation of HXK2, c-Myc also contributes

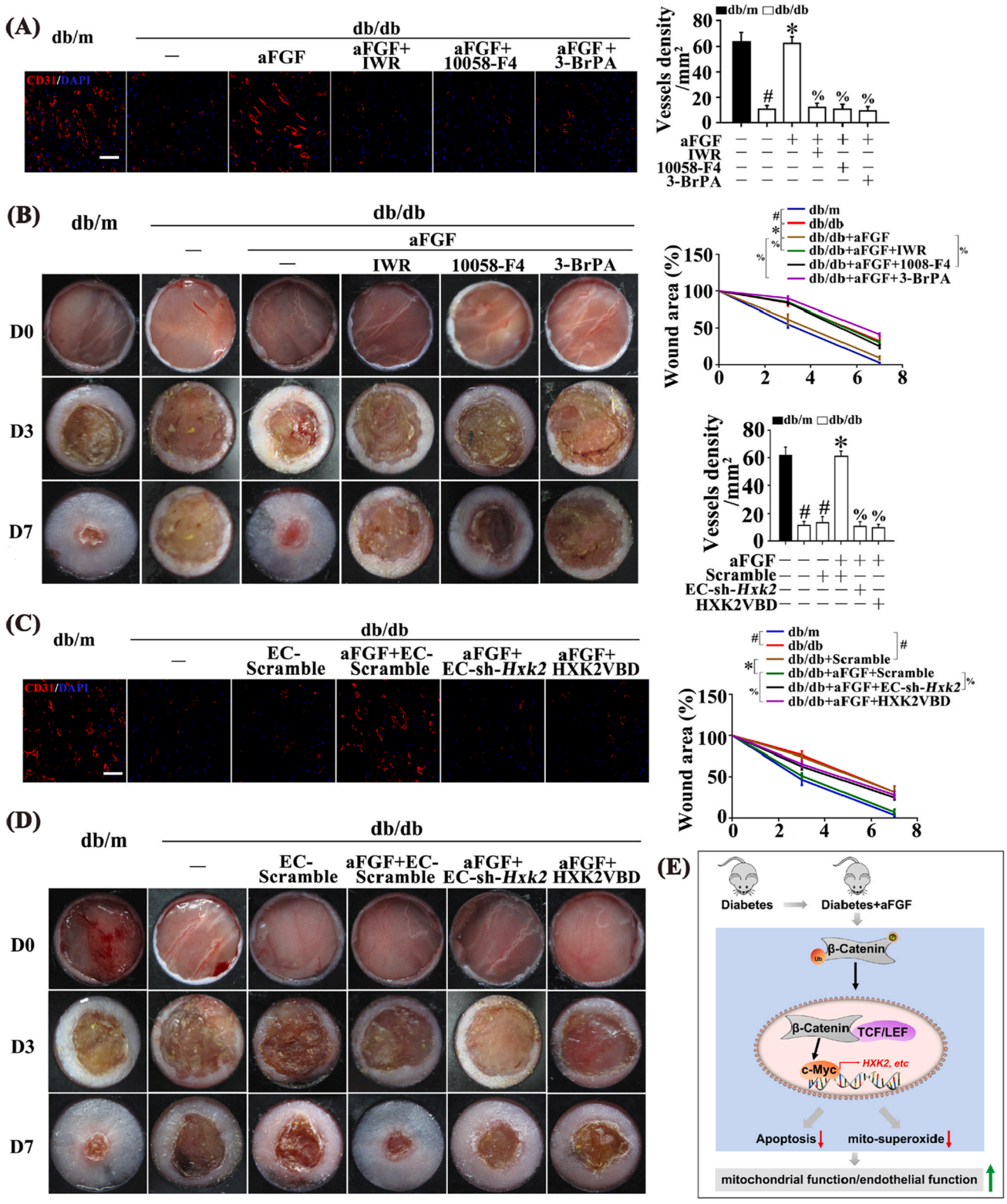

Fig. 7. Inhibition of Wnt/β-catenin-c-Myc-HXK2 pathway and/or interference with mitochondrial location of HXK2 abrogated aFGF-prompted wound healing in T2DM. (**A**) Confocal immunofluorescence staining with CD31 of wounded skin tissue sections at 7 days post wounding, scale bars = 30 μm, and (**B**) Images of skin wounds from db/m mice, db/db mice and db/db mice receiving aFGF (100 ng/mL) treatment. For signaling pathway analysis, ICG-001 (10 μM) or 10058-F4 (50 μM) or BrPA (50 μM) was injected intradermally into the wound edges in the mice after aFGF treatment. (**C**) Confocal immunofluorescence staining with CD31 of wounded skin tissue sections at 7 days post wounding, scale bars = 30 μm, and (**D**) images of skin wounds from db/m mice, db/db mice and db/db mice receiving aFGF (100 ng/mL) treatment. Ad-sh-*HXK2* was injected intradermally into the wound edges in the mice the day before wounding, HXK2VBD peptide (100 μM) was injected intradermally into the wound edges in the mice after aFGF treatment. (**E**) Schematic showing that aFGF alleviated diabetes-induced endothelial impairment by downregulating mtROS via Wnt/β-catenin pathway. All values displayed are means ± SEM of 6 independent experiments. #$p < 0.05$ vs. db/m mice; *$p < 0.05$ vs. db/db mice; % $p < 0.05$ vs. aFGF treated db/db mice.

to association of HXK2 with mitochondrial VDAC [45]. Clinical investigations revealed that HXK2 protein levels are decreased in human coronary ECs (HCECs) from diabetic patients relative to HCECs from non-diabetic patients. Further experimental studies confirmed the finding that HG treatment significantly decreases HXK2 protein levels in mouse coronary ECs (MCECs), while HXK2 overexpression in MCECs derived from diabetic mice decreases mtROS production [62]. Therefore, in the present study, we investigated whether aFGF modulated the c-Myc/HXK2 axis in ECs, and the role of this interaction in aFGF-mediated endothelial protection. aFGF mediated upregulation of HXK2 expression in a c-Myc-dependent manner. To elucidate the roles of HXK2 in the endothelial protective effects of aFGF in HG + PA conditions, we used si-*Hxk2* to disrupt expression of HXK2 and used HXK2VBD to disrupt mitochondrial localization of HXK2 in HUVECs. Both silencing of HXK2 and dissociation of HXK2 from mitochondria largely abolished the endothelial protective effects of aFGF. This result was further confirmed using the HXK2 inhibitor 3-BrPA in *db/db* mice, which abolished the protective effects of aFGF in aortic ECs.

Impaired angiogenesis is a crucial factor impeding the wound healing process in diabetes [63]. Wound healing is a complex, dynamic, and highly controlled process, in which angiogenesis plays a crucial role in nourishing newly formed tissues. Vascular ECs play an important role in angiogenesis and contribute to the wound healing process [64]. However, endothelial dysfunction is an early and fundamental pathological change in diabetes [65]. The present study demonstrated that aFGF upregulated expression of HXK2 and c-Myc, promoting angiogenesis and wound healing in *db/db* mice. This effect was abrogated by co-treatment with IWR, 10058-F4, and 3-BrPA, which inhibit Wnt/β-catenin, c-Myc, and HXK2, respectively. Moreover, these results were further confirmed by silencing HXK2 and dissociating HXK2 from the mitochondria, which largely abolished aFGF promotion of angiogenesis and wound healing.

5. Conclusion

Collectively, our data demonstrated for the first time that the protective effects of aFGF in diabetes-induced endothelial impairment can be attributed mainly to its role in activating the Wnt/β-catenin signaling pathway, and the resultant alleviation of mitochondrial oxidative stress. Moreover, we revealed that alleviation of diabetic mitochondrial oxidative stress by aFGF-mediated Wnt/β-catenin signaling pathway activation was c-Myc dependent, and involved HXK2. The present study established a novel role for aFGF in endothelial protection in diabetes, which was due to alleviation of mitochondrial oxidative stress. These findings provide new insights into the pathogenesis and treatment of diabetic vascular complications.

Funding

This work was supported by the National Natural Science Foundation of China [grant numbers 81903235, 81870209, 81773346, 81770498, 82070507], the Key Scientific Project of MOST, China (grant number 2017YFA0506000), the Natural Science Foundation of Zhejiang Province [grant number LQ18H020004, Y21H020057], Zhejiang Province Medical and Health Science Program [grant number 2019KY099, 2019RC054], and the Wenzhou Science and Technology Bureau Foundation [grant numbers Y20180145, Y20190164].

Declaration of competing interest

The authors declare that they have no known competing financial interests or personal relationships that could have appeared to influence the work reported in this paper.

Appendix A. Supplementary data

Supplementary data to this article can be found online at https://doi.org/10.1016/j.redox.2020.101811.

References

[1] L. Xiang, P.N. Mittwede, J.S. Clemmer, Glucose homeostasis and cardiovascular alterations in diabetes, Comp. Physiol. 5 (4) (2015) 1815–1839, https://doi.org/10.1002/cphy.c150001. Published 2015 Sep. 20.
[2] M.A. Kluge, J.L. Fetterman, J.A. Vita, Mitochondria and endothelial function, Circ. Res. 112 (8) (2013) 1171–1188, https://doi.org/10.1161/CIRCRESAHA.111.300233.
[3] C.M. Hoyos, K.L. Melehan, P.Y. Liu, R.R. Grunstein, C.L. Phillips, Does obstructive sleep apnea cause endothelial dysfunction? A critical review of the literature, Sleep Med. Rev. 20 (2015) 15–26, https://doi.org/10.1016/j.smrv.2014.06.003.
[4] Y.M. Kim, S.W. Youn, V. Sudhahar, et al., Redox regulation of mitochondrial fission protein drp1 by protein disulfide isomerase limits endothelial senescence, Cell Rep. 23 (12) (2018) 3565–3578, https://doi.org/10.1016/j.celrep.2018.05.054.
[5] M. Quintero, S.L. Colombo, A. Godfrey, S. Moncada, Mitochondria as signaling organelles in the vascular endothelium, Proc. Natl. Acad. Sci. U. S. A. 103 (14) (2006) 5379–5384, https://doi.org/10.1073/pnas.0601026103.
[6] A.C. Bayne, R.J. Mockett, W.C. Orr, R.S. Sohal, Enhanced catabolism of mitochondrial superoxide/hydrogen peroxide and aging in transgenic Drosophila, Biochem. J. 391 (Pt 2) (2005) 277–284, https://doi.org/10.1042/BJ20041872.
[7] M. Brownlee, The pathobiology of diabetic complications: a unifying mechanism, Diabetes 54 (6) (2005) 1615–1625, https://doi.org/10.2337/diabetes.54.6.1615.
[8] M. Brownlee, Biochemistry and molecular cell biology of diabetic complications, Nature 414 (6865) (2001) 813–820, https://doi.org/10.1038/414813a.
[9] J.L. Evans, I.D. Goldfine, B.A. Maddux, G.M. Grodsky, Oxidative stress and stress-activated signaling pathways: a unifying hypothesis of type 2 diabetes, Endocr. Rev. 23 (5) (2002) 599–622, https://doi.org/10.1210/er.2001-0039.
[10] J.M. Li, A.M. Shah, Endothelial cell superoxide generation: regulation and relevance for cardiovascular pathophysiology, Am. J. Physiol. Regul. Integr. Comp. Physiol. 287 (5) (2004) R1014–R1030, https://doi.org/10.1152/ajpregu.00124.2004.
[11] I. Fridovich, Superoxide radical and superoxide dismutases, Annu. Rev. Biochem. 64 (1995) 97–112, https://doi.org/10.1146/annurev.bi.64.070195.000525.
[12] W. Yang, D.P. de Bono, A new role for vascular endothelial growth factor and fibroblast growth factors: increasing endothelial resistance to oxidative stress, FEBS Lett. 403 (2) (1997) 139–142, https://doi.org/10.1016/s0014-5793(96)01486-x.
[13] Y. Nagayasu, S.Y. Morita, H. Hayashi, et al., Increasing cellular level of phosphatidic acid enhances FGF-1 production in long term-cultured rat astrocytes, Brain Res. 1563 (2014) 31–40, https://doi.org/10.1016/j.brainres.2014.03.035.
[14] J.I. Ito, Y. Nagayasu, T. Ogawa, H. Okihara, M. Michikawa, Biochemical properties in membrane of rat astrocytes under oxidative stress, Brain Res. 1615 (2015) 1–11, https://doi.org/10.1016/j.brainres.2015.04.008.
[15] W. Yang, D.P. de Bono, A new role for vascular endothelial growth factor and fibroblast growth factors: increasing endothelial resistance to oxidative stress, FEBS Lett. 403 (2) (1997) 139–142, https://doi.org/10.1016/s0014-5793(96)01486-x.
[16] G. Liang, L. Song, Z. Chen, et al., Fibroblast growth factor 1 ameliorates diabetic nephropathy by an anti-inflammatory mechanism, Kidney Int. 93 (1) (2018) 95–109, https://doi.org/10.1016/j.kint.2017.05.013.
[17] S.R. Martins-Neves, D.I. Paiva-Oliveira, C. Fontes-Ribeiro, J.V.M.G. Bovée, A. M. Cleton-Jansen, C.M.F. Gomes, IWR-1, a tankyrase inhibitor, attenuates Wnt/β-catenin signaling in cancer stem-like cells and inhibits in vivo the growth of a subcutaneous human osteosarcoma xenograft, Canc. Lett. 414 (2018) 1–15, https://doi.org/10.1016/j.canlet.2017.11.004.
[18] W.R. Henderson Jr., E.Y. Chi, X. Ye, et al., Inhibition of Wnt/beta-catenin/CREB binding protein (CBP) signaling reverses pulmonary fibrosis, Proc. Natl. Acad. Sci. U. S. A. 107 (32) (2010) 14309–14314, https://doi.org/10.1073/pnas.1001520107.
[19] X. Wang, L. Sun, X. Wang, et al., Acidified bile acids enhance tumor progression and telomerase activity of gastric cancer in mice dependent on c-Myc expression, Cancer Med. 6 (4) (2017) 788–797, https://doi.org/10.1002/cam4.999.
[20] K. Birsoy, T. Wang, R. Possemato, et al., MCT1-mediated transport of a toxic molecule is an effective strategy for targeting glycolytic tumors, Nat. Genet. 45 (1) (2013) 104–108, https://doi.org/10.1038/ng.2471.
[21] D. Li, A. Wang, X. Liu, et al., MicroRNA-132 enhances transition from inflammation to proliferation during wound healing, J. Clin. Invest. 125 (8) (2015) 3008–3026, https://doi.org/10.1172/JCI79052.
[22] M. Baker, S.D. Robinson, T. Lechertier, et al., Use of the mouse aortic ring assay to study angiogenesis, Nat. Protoc. 7 (1) (2011) 89–104, https://doi.org/10.1038/nprot.2011.435. Published 2011 Dec 22.
[23] A.C. Aplin, R.F. Nicosia, The rat aortic ring model of angiogenesis, Methods Mol. Biol. 1214 (2015) 255–264, https://doi.org/10.1007/978-1-4939-1462-3_16.
[24] D. Schuler, R. Sansone, T. Freudenberger, et al., Measurement of endothelium-dependent vasodilation in mice–brief report, Arterioscler. Thromb. Vasc. Biol. 34 (12) (2014) 2651–2657, https://doi.org/10.1161/ATVBAHA.114.304699.
[25] H. Wang, W. Luo, J. Wang, et al., Obesity-induced endothelial dysfunction is prevented by deficiency of P-selectin glycoprotein ligand-1, Diabetes 61 (12) (2012) 3219–3227, https://doi.org/10.2337/db12-0162.
[26] H.A. Itani, A.E. Dikalova, W.G. McMaster, et al., Mitochondrial cyclophilin D in vascular oxidative stress and hypertension, Hypertension 67 (6) (2016) 1218–1227, https://doi.org/10.1161/HYPERTENSIONAHA.115.07085.

[27] S. Dikalov, K.K. Griendling, D.G. Harrison, Measurement of reactive oxygen species in cardiovascular studies, Hypertension 49 (4) (2007) 717–727, https://doi.org/10.1161/01.HYP.0000258594.87211.6b.
[28] S. Rikka, M.N. Quinsay, R.L. Thomas, et al., Bnip3 impairs mitochondrial bioenergetics and stimulates mitochondrial turnover, Cell Death Differ. 18 (4) (2011) 721–731, https://doi.org/10.1038/cdd.2010.146.
[29] J. Magalhães, I. Falcão-Pires, I.O. Gonçalves, et al., Synergistic impact of endurance training and intermittent hypobaric hypoxia on cardiac function and mitochondrial energetic and signaling, Int. J. Cardiol. 168 (6) (2013) 5363–5371, https://doi.org/10.1016/j.ijcard.2013.08.001.
[30] P. Dromparis, E.D. Michelakis, Mitochondria in vascular health and disease, Annu. Rev. Physiol. 75 (2013) 95–126, https://doi.org/10.1146/annurev-physiol-030212-183804.
[31] A. Czajka, S. Ajaz, L. Gnudi, et al., Altered mitochondrial function, mitochondrial DNA and reduced metabolic flexibility in patients with diabetic nephropathy, EBioMedicine 2 (6) (2015) 499–512, https://doi.org/10.1016/j.ebiom.2015.04.002. Published 2015 Apr 11.
[32] F. Giacco, M. Brownlee, Oxidative stress and diabetic complications, Circ. Res. 107 (9) (2010) 1058–1070, https://doi.org/10.1161/CIRCRESAHA.110.223545.
[33] X. Cheng, R.C. Siow, G.E. Mann, Impaired redox signaling and antioxidant gene expression in endothelial cells in diabetes: a role for mitochondria and the nuclear factor-E2-related factor 2-Kelch-like ECH-associated protein 1 defense pathway, Antioxidants Redox Signal. 14 (3) (2011) 469–487, https://doi.org/10.1089/ars.2010.3283.
[34] A.E. Dikalova, A.T. Bikineyeva, K. Budzyn, et al., Therapeutic targeting of mitochondrial superoxide in hypertension, Circ. Res. 107 (1) (2010) 106–116, https://doi.org/10.1161/CIRCRESAHA.109.214601.
[35] S.I. Dikalov, R.R. Nazarewicz, A. Bikineyeva, et al., Nox2-induced production of mitochondrial superoxide in angiotensin II-mediated endothelial oxidative stress and hypertension, Antioxidants Redox Signal. 20 (2) (2014) 281–294, https://doi.org/10.1089/ars.2012.4918.
[36] L. Jiang, M. Yin, X. Wei, et al., Bach1 Represses Wnt/β-Catenin Signaling and Angiogenesis [published correction appears in Circ Res. 2015 Oct 9;117(9):e79], Circ. Res. 117 (4) (2015) 364–375, https://doi.org/10.1161/CIRCRESAHA.115.306829.
[37] A. Muley, S. Majumder, G.K. Kolluru, et al., Secreted frizzled-related protein 4: an angiogenesis inhibitor, Am. J. Pathol. 176 (3) (2010) 1505–1516, https://doi.org/10.2353/ajpath.2010.090465.
[38] L. Wang, L. Qing, H. Liu, et al., Mesenchymal stromal cells ameliorate oxidative stress-induced islet endothelium apoptosis and functional impairment via Wnt4-β-catenin signaling, Stem Cell Res. Ther. 8 (1) (2017) 188, https://doi.org/10.1186/s13287-017-0640-0. Published 2017 Aug 14.
[39] R. Nusse, H. Clevers, Wnt/β-Catenin signaling, disease, and emerging therapeutic modalities, Cell 169 (6) (2017) 985–999, https://doi.org/10.1016/j.cell.2017.05.016.
[40] F.I. Lu, Y.H. Sun, C.Y. Wei, C. Thisse, B. Thisse, Tissue-specific derepression of TCF/LEF controls the activity of the Wnt/β-catenin pathway, Nat. Commun. 5 (2014) 5368, https://doi.org/10.1038/ncomms6368. Published 2014 Nov 5.
[41] F. De Nigris, L.O. Lerman, M. Condorelli, A. Lerman, C. Napoli, Oxidation-sensitive transcription factors and molecular mechanisms in the arterial wall, Antioxidants Redox Signal. 3 (6) (2001) 1119–1130, https://doi.org/10.1089/152308601317203620.
[42] P. Ahuja, P. Zhao, E. Angelis, et al., Myc controls transcriptional regulation of cardiac metabolism and mitochondrial biogenesis in response to pathological stress in mice, J. Clin. Invest. 120 (5) (2010) 1494–1505, https://doi.org/10.1172/JCI38331.
[43] K. Wilhelm, K. Happel, G. Eelen, et al., FOXO1 couples metabolic activity and growth state in the vascular endothelium, Nature 529 (7585) (2016) 216–220, https://doi.org/10.1038/nature16498.
[44] R. Mair, A.J. Wright, S. Ros, et al., Metabolic imaging detects low levels of glycolytic activity that vary with levels of c-myc expression in patient-derived xenograft models of glioblastoma, Canc. Res. 78 (18) (2018) 5408–5418, https://doi.org/10.1158/0008-5472.CAN-18-0759.
[45] M.A. Al-Zeer, A. Xavier, M. Abu Lubad, et al., Chlamydia trachomatis prevents apoptosis via activation of PDPK1-MYC and enhanced mitochondrial binding of hexokinase II, EBioMedicine 23 (2017) 100–110, https://doi.org/10.1016/j.ebiom.2017.08.005.
[46] G. Viticchiè, M. Agostini, A.M. Lena, et al., p63 supports aerobic respiration through hexokinase II, Proc. Natl. Acad. Sci. U. S. A. 112 (37) (2015) 11577–11582, https://doi.org/10.1073/pnas.1508871112.
[47] A.S. Antonopoulos, G. Siasos, T. Konsola, et al., Arterial wall elastic properties and endothelial dysfunction in the diabetic foot syndrome in patients with type 2 diabetes, Diabetes Care 38 (11) (2015) e180–e181, https://doi.org/10.2337/dc15-1042.
[48] Advance Collaborative Group, A. Patel, S. MacMahon, et al., Intensive blood glucose control and vascular outcomes in patients with type 2 diabetes, N. Engl. J. Med. 358 (24) (2008) 2560–2572, https://doi.org/10.1056/NEJMoa0802987.
[49] L.F. Fried, N. Emanuele, J.H. Zhang, et al., Combined angiotensin inhibition for the treatment of diabetic nephropathy [published correction appears in N Engl J Med. 2014;158:A7255], N. Engl. J. Med. 369 (20) (2013) 1892–1903, https://doi.org/10.1056/NEJMoa1303154.
[50] A.M. Lincoff, S.J. Nicholls, J.S. Riesmeyer, et al., Evacetrapib and cardiovascular outcomes in high-risk vascular disease, N. Engl. J. Med. 376 (20) (2017) 1933–1942, https://doi.org/10.1056/NEJMoa1609581.
[51] F. Paneni, S. Costantino, L. Castello, et al., Targeting prolyl-isomerase Pin1 prevents mitochondrial oxidative stress and vascular dysfunction: insights in patients with diabetes, Eur. Heart J. 36 (13) (2015) 817–828, https://doi.org/10.1093/eurheartj/ehu179.
[52] L. Zhang, C. Yu, F.E. Vasquez, et al., Hyperglycemia alters the schwann cell mitochondrial proteome and decreases coupled respiration in the absence of superoxide production, J. Proteome Res. 9 (1) (2010) 458–471, https://doi.org/10.1021/pr900818gz.
[53] M. Kostas, A. Lampart, J. Bober, et al., Translocation of exogenous FGF1 and FGF2 protects the cell against apoptosis independently of receptor activation, J. Mol. Biol. 430 (21) (2018) 4087–4101, https://doi.org/10.1016/j.jmb.2018.08.004.
[54] M. Skibba, C. Zhang, X. Jiang, Y. Xin, L. Cai, Preventive effect of non-mitogenic acidic fibroblast growth factor on diabetes-induced testicular cell death, Reprod. Toxicol. 49 (2014) 136–144, https://doi.org/10.1016/j.reprotox.2014.08.002.
[55] Y.Z. Zhao, M. Zhang, H.L. Wong, et al., Prevent diabetic cardiomyopathy in diabetic rats by combined therapy of aFGF-loaded nanoparticles and ultrasound-targeted microbubble destruction technique, J. Contr. Release 223 (2016) 11–21, https://doi.org/10.1016/j.jconrel.2015.12.030.
[56] S. Foulquier, E.P. Daskalopoulos, G. Lluri, K.C.M. Hermans, A. Deb, W. M. Blankesteijn, WNT signaling in cardiac and vascular disease, Pharmacol. Rev. 70 (1) (2018) 68–141, https://doi.org/10.1124/pr.117.013896.
[57] N. Lehwald, G.Z. Tao, K.Y. Jang, M. Sorkin, W.T. Knoefel, K.G. Sylvester, Wnt-β-catenin signaling protects against hepatic ischemia and reperfusion injury in mice, Gastroenterology 141 (2) (2011) 707–718, https://doi.org/10.1053/j.gastro.2011.04.051, e7185.
[58] L. Qian, J. Hong, Y. Zhang, et al., Downregulation of S100A4 alleviates cardiac fibrosis via Wnt/β-catenin pathway in mice, Cell. Physiol. Biochem. 46 (6) (2018) 2551–2560, https://doi.org/10.1159/000489683.
[59] L. Li, Y. Dang, J. Zhang, et al., REGγ is critical for skin carcinogenesis by modulating the Wnt/β-catenin pathway, Nat. Commun. 6 (2015) 6875, https://doi.org/10.1038/ncomms7875. Published 2015 Apr 24.
[60] K.C. Sedoris, S.D. Thomas, C.R. Clarkson, et al., Genomic c-Myc quadruplex DNA selectively kills leukemia, Mol. Canc. Therapeut. 11 (1) (2012) 66–76, https://doi.org/10.1158/1535-7163.MCT-11-0515.
[61] P. Yu, K. Wilhelm, A. Dubrac, et al., FGF-dependent metabolic control of vascular development, Nature 545 (7653) (2017) 224–228, https://doi.org/10.1038/nature22322.
[62] M. Pan, Y. Han, A. Basu, et al., Overexpression of hexokinase 2 reduces mitochondrial calcium overload in coronary endothelial cells of type 2 diabetic mice, Am. J. Physiol. Cell Physiol. 314 (6) (2018) C732–C740, https://doi.org/10.1152/ajpcell.00350.2017.
[63] M. Ackermann, A.M. Pabst, J.P. Houdek, T. Ziebart, M.A. Konerding, Priming with proangiogenic growth factors and endothelial progenitor cells improves revascularization in linear diabetic wounds, Int. J. Mol. Med. 33 (4) (2014) 833–839, https://doi.org/10.3892/ijmm.2014.1630.
[64] N. Sawada, A. Jiang, F. Takizawa, et al., Endothelial PGC-1α mediates vascular dysfunction in diabetes, Cell Metabol. 19 (2) (2014) 246–258, https://doi.org/10.1016/j.cmet.2013.12.014.
[65] D.H. Wasserman, T.J. Wang, N.J. Brown, The vasculature in prediabetes, Circ. Res. 122 (8) (2018) 1135–1150, https://doi.org/10.1161/CIRCRESAHA.118.311912.